Politecnico di Torino

Master's Degree in Environmental and Land Engineering
Climate Change
A.Y. 2023/2024
Exam session March/2024

Hydrological response to meteorological drought in southern Piedmont

Thesis advisor:

Alberto Viglione

Co-advisor:

Emanuele Mombrini

Candidate:

Fabiola Cannizzaro

Abstract

This study aims at characterizing the response of hydrological basins of southern Piedmont (Italy) to meteorological drought that, through the "propagation" process, can evolve in hydrological drought, causing several damages to the economic and social sectors. More specifically, in this work we detect the correlation between meteorological and hydrological drought on a basin scale for catchments of different size. We select three direct tributaries of the Po River in southern Piedmont: Varaita, Maira and Tanaro rivers, the latter being much wider than the first two. First, we quantify the severity of the meteorological and hydrological droughts as independent phenomena, through the computation of two standardized indexes for the three basins from the last years of the 1990s to 2022 (availability of data). To identify meteorological droughts, we exploit the Arpa Piemonte dataset NWOI, with a 0.125 resolution, containing daily precipitation, daily maximum and minimum temperature, and calculate the monthly Standardized Precipitation Evapotranspiration Index (SPEI) for 1, 3, 6, 9, 12 and 24 months aggregation periods. The SPEI's are then averaged on the areas of the three basins, achieving a single monthly value for each catchment and aggregation period. To identify hydrological droughts, we consider the gauging stations located at the closing section of each basin, and we use the Standardized Streamflow Index (SSI). To calculate SSI, the capability of five probability distributions to represent all monthly streamflow data is quantified and tested through goodness-of-fit tests. Among all tested distribution, the log-logistic is chosen since it shows a good fit for all the monthly series. Once the monthly series of SPEI and SSI is obtained for each catchment, a correlation analysis is set by using the Pearson coefficient, both on the whole period and on a monthly scale. The results show a high positive correlation for all the aggregation periods. Interestingly, and unexpectedly, the highest correlation is detected for 6 months and 24 months for the Varaita and Maira catchments and for 3 months aggregation period for the Tanaro basin, even though the correlation remains higher than 0.6 even for longer timescales. The hydrological response of the first two catchments is similar, as expected, since they are medium-high slope mountainous basins with fast response in the short time scale, showing unexpectedly a good memory for the response associated to the long-time scales. The Tanaro basin responds to short and medium time scale in autumn and winter, presenting a lower correlation in the long-time scale. The reasons for the difference in the timescales characterizing the propagation from meteorological to hydrological droughts should be investigated by expanding the analysis on more catchments characterized by different climatic and hydrological regimes.

Table of contents

1. Introduction

Drought can be classified as a natural hazard, such as floods, hurricanes, storms, tornadoes, volcanic eruptions, and earthquakes. What differentiates drought from other phenomena is that it is considered as a "creeping disaster", because it is slow and insidious, spanning wide and not well circumscribed areas. Unlike floods events, understanding the duration and magnitude of drought periods is not easy (spanning from months to years). Drought can have repercussions on the environment and society also after its occurrence, and this depends both on environmental and social-economic aspects. The recovery time and criticality of drought events can vary from region to region. In developing countries drought events have often devastating effects, (high vulnerability to drought), not only because of their geography but also because of their economic system mainly based on agricultural sector. These premises let us understand that this is one of the most destructive natural hazards [Wilhite, 2000], affecting several economic sectors, such as drinking water supply, crop production, electricity production. What is generated is a chain reaction in societal challenges, leading to food shortages, large-scale migration, and loss of life.

The Mediterranean basin and specifically northern Italy are recognised as climate change hotspots, where extreme events (i.e., heat waves, floods, droughts etc) increase their frequency and duration. As stated in the AR6, Chapter 4, by IPCC, droughts have become more frequent and intense, especially in the north Mediterranean (high confidence), and, according to the IPCC (AR6, Chapter 13), it is expected an increase in risk from drought in Southern Europe, being high by mid-century and very high by the end of the century compared with the baseline (1995–2014).

Given that the Alps region is one of the main areas where climate change effects will be more evident, especially concerning the alteration of the hydrological cycle, this thesis has the purpose to analyse the region response to drought periods, by examining historical trends. This study is expected to contribute to the development of local adaptation strategies in water management for the next future. More specifically, the goal of this work is to find a correlation between climatic and hydrological drought in the south of Piedmont, specifically in Cuneo, Asti, and Alessandria provinces. The problem of drought has acquired relevance in Piedmont in the last 50 years during which it has been observed an increase in the frequency and duration of drought periods (Arpa Piemonte). This has led to several problems in water management, especially in the agriculture sector and in the production of hydropower. To assess the response of drainage areas to prolonged periods of drought ("Propagation drought"), a statistical analysis has been set, aiming at studying the correlation between two types of droughts: meteorological and hydrological drought, respectively quantified by the *Standardized Precipitation Evapotranspiration Index* (SPEI) and of the *Standardized Streamflow Index* (SSI). The first chapter focuses on the description of different types of droughts and on their qualitative characterization, followed by a zoom on Piedmont local drought conditions since the half of last century and a brief discussion on possible future scenarios. The second introductive chapter is dedicated to the meteorological description of southern Piedmont area and on the selection of catchments of direct tributaries of Po River, each of which is individually studied and described based on its morphological characteristics. The third chapter focuses on the methodology followed to quantify the correlation coefficient between SPEI and SSI. Using the NWOI gridded dataset from Arpa Piemonte, containing historical daily series of precipitation, maximum and minimum temperature, it is possible to quantify the SPEI index on a basin scale. Subsequently, the hydrometric stations at the closing sections of each drainage area are identified to assess the hydrological condition of the main fluvial channel of the catchment and, thus, to compute the SSI. Finally, the correlation among the SSI and SPEI for each basin is computed. To conclude, the last chapter regards the results and the possible considerations on the output found out from the whole analysis, comprehending the observation of possible temporal trends, analysing the time lag between climatic and hydrological drought, and if present, the attenuation, pooling, and lengthening effects. The final goal is to understand the relationship between meteorological and hydrological droughts and how long it takes to observe water deficit effects on superficial water bodies.

1.1 Drought definition

Drought is a complex phenomenon and, therefore, it has been defined in many ways. It is a persistent and extended condition of deficit of water with respect to normal conditions. The adjective "normal" can be difficult to interpret as it depends on what water is used for. In this study we consider the definition by Tallaksen and Van Lanen (2004):

"Drought is a sustained period of below-normal water availability. It is a recurring and worldwide phenomenon, with spatial and temporal characteristics that vary significantly from one region to another."

Drought can be divided in four general categories (Van Loon, 2015):

- **Meteorological drought[1]:** deficit of precipitation, combined with an increase in evapotranspiration extended in a large area and for a long period of time.
- **Soil moisture drought:** deficit in soil moisture, specifically in the root zone. It is related to the failure of crop and vegetation (also called agricultural drought).
- **Hydrological drought:** deficit of surface and subsurface water: negative anomalies in groundwater levels, lakes, and river discharge.
- **Socioeconomic drought:** impacts of the three mentioned droughts categories and it is related to deficit of water for social needs or for economic sectors (e.g., agriculture).

The above-mentioned four categories can be seen in a system of driver-impact processes, well explained by Figure 1-1.

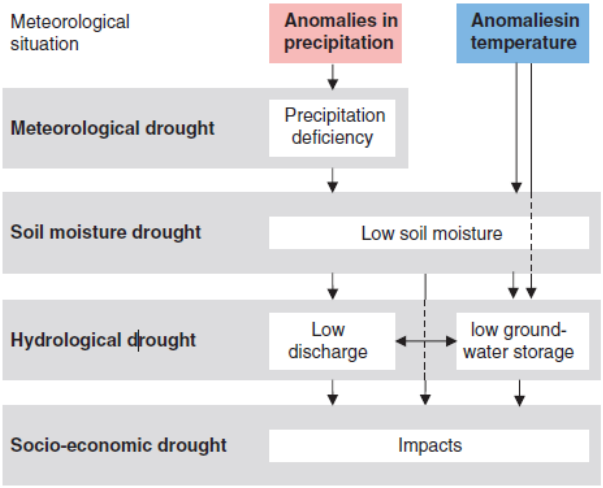

Figure 1-1 Scheme representing different categories of drought and their development. (Derived from Peters,53 Van Loon,54 Stahl55). (Van Loon, 2015)

As said before it is hard to recognize the onset, the extent, and the end of a drought periods and to quantify its severity, duration, magnitude, and spatial extent.

It has been spent a lot of effort and time by researchers to develop indexes that accurately quantify the severity of climatic drought. Examples of the most used indexes are the Palmer Drought Severity Index (PDSI) (Palmer, 1965), the Standardized Precipitation Index (SPI) (McKee et al., 1993), the Standardized Precipitation-Evapotranspiration Index (SPEI) (Vicente-Serrano et al., 2010a) and the Soil Moisture Deficit Index (SMDI) (Narasimhan and Srinivasan, 2005). The major key feature of meteorological drought indexes is that they allow to compare the severity of the events in different locations independently from the local climatic characteristics (Vicente-Serrano et al. 2011). Hence, the methodologies for quantifying climate drought conditions are

[1] In this study the use of the terms: "meteorological drought" and "climatic drought" is equivalent

typically derived using standardized series of hydroclimatic variables of interest. Following this method, the cumulative distribution function is employed corresponding to each value of the hydroclimatic variable of interest.

Hydrological drought can be assessed as an independent phenomenon, even if it prevalently originates from climatic drought. Traditionally, studies on hydrological drought rely on the “run theory”, considering deviations from a truncation level during a defined period. However, this method faces limitations due to seasonality and hampers comparisons between different basins. Challenges mainly arise from the spatial variability influenced by factors like topography, lithology, reservoirs, and vegetation. This is the reason why researchers have spent efforts in developing standardized indexes which could describe the severity of hydrological drought events. In this study we exploit the methodology implemented by Vicente-Serrano in the publication titled "Accurate computation of a streamflow drought index" in 2011, who developed the Standardized Streamflow Index (SSI).

In this work the SPEI and SSI have been computed on a basin scale to describe respectively climatic and hydrological drought, following the Vicente-Serrano approach in “Hydrological response to climate variability at different time scales: A study in the Ebro basin” of 2011. The methodology used to compute both indexes is accurately explained in Chapter 3.

1.2 Drought propagation

The translation from anomalous meteorological conditions to hydrological drought has been called “drought propagation” (Eltahir and Yeh, 1999). This term summarizes the effects that precipitation deficits and anomalies in temperature have on the terrestrial part of the hydrological cycle (i.e., soil moisture, runoff, recharge, groundwater, and discharge).

River streamflow is a combination of fast-flow (runoff) and base-flow (groundwater discharge). During a long dry spell combined with an increase in evapotranspiration, the runoff immediately decreases, followed by a progressive reduction of soil moisture. During these events, superficial streamflow consequently decreases being fed mainly only by slow pathways of groundwater discharge. Usually, the last compartment of the hydrological terrestrial cycle being affected by meteorological drought is the groundwater, that effectively diminishes if the dry period persists over time, for example after a multi-year drought. (Figure 1-2)

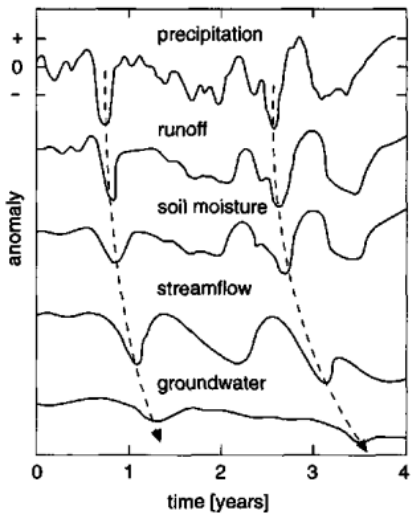

Figure 1-2 Propagation of rainfall anomalies through sub-surface reservoirs (Kim, 1995)

The terrestrial part of the hydrological cycle acts as a "low-pass filter to the meteorological forcing, adding memory to the system" (Kim, 1995). The main features commonly detected in propagation drought process are described below and graphically explained in Figure 1-3 (Van Loon, 2015):

- **Pooling:** climatic consecutive droughts are combined into a prolonged hydrological drought.
- **Attenuation:** meteorological droughts are attenuated in the stores, causing a smoothing of the maximum negative anomaly.
- **Lag:** a lag occurs between meteorological, soil moisture, and hydrological drought, i.e., the timing of the onset is later when moving through the hydrological cycle.
- **Lengthening:** droughts last longer when moving from meteorological drought via soil moisture drought to hydrological drought (longer memory).

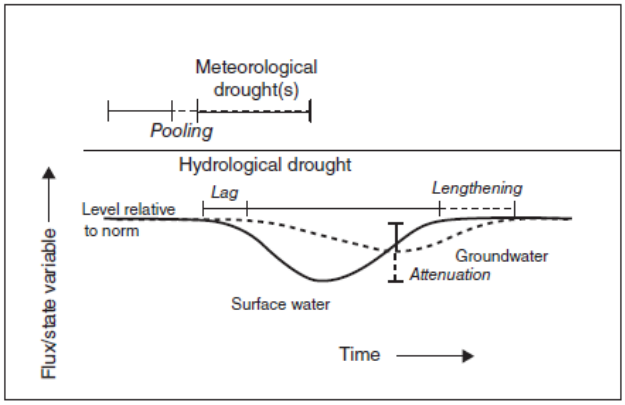

Figure 1-3 Features characterizing the propagation of meteorological drought(s) to hydrological drought: pooling, lag, attenuation, and lengthening. (Reprinted with permission from Hisdal and Tallaksen109) (Van Loon, 2015)

Hydrological drought is a complex result of nonlinear interactions between climate and catchment processes (Konapala et al., 2020). Lag and attenuation are only dependent on catchment control, pooling, and lengthening both by climate and catchment control.

1.2.1 Climate control on hydrological process

Climate is the driver of terrestrial hydrological process, which is strongly dependent on the input of multiple variables, such as precipitation, snow, and temperature. Climate regimes vary around the world, but all types of climates[2] can be affected by drought. Based on the diversity of climatic drought as a causative mechanism, the process of drought propagation leads to different types of hydrological droughts (Van Loon and Van Lanen, 2012):

- *Classical rainfall deficit drought:* it is caused only by a prolonged dry period (no rainfall - meteorological drought) that translates into a hydrological drought through the hydrological cycle. It is usually recurrent in constant climates (VanLoon, 2015), but it can be observed in any climate region (Köppen and Geiger classification, A, B, C, D and E, except for H) and both in catchments with fast and slow responding and can show all the features described above: pooling, attenuation, lag, and lengthening.
- *Rain-to-snow-season drought:* Lack of rainfall during wet season (usually summer/autumn) that persists also in the cold season (winter). The below "normal" level of soil moisture and groundwater storage causes a reduction of discharge. Only in the snow melt season, groundwater storage will be replenished, and recharge condition restored (spring). This type of hydrological drought can occur in climates type D and E, and some subtypes of C and presents all drought propagation features with an accentuated lengthening effect.

[2] Köppen-Geiger climate types classification

- *Wet-to-dry-season drought:* In seasonal climates, it is generated by "below-normal" precipitation during the wet season (usually winter). Meteorological drought also persists during the dry season (summer), when it is exacerbated by a higher rate of evapotranspiration. The starting conditions of soil moisture and groundwater level in summer are below the normal values, leading to decrease in discharge levels (hydrological drought). This happens for example in C-Mediterranean climates with an accentuated lengthening effect.
- *Cold snow season drought:* it is caused by well-below zero temperature in the snow season (winter), leading to premature beginning of snow accumulation and/or late snow melt (no groundwater recharge in those periods) possibly, but not necessarily, combined with a meteorological drought in that same season. Occurrence usually in C, D and E climates.
- *Warm snow season drought*: it is caused by much higher temperature than "normal" condition in the snow season (winter), in some cases combined with precipitation deficit (meteorological drought) in the season. It can occur in climates with well-below zero temperature in winter, generating late snow formation and/or premature snow melt, or in climates with around zero temperature in winter, causing occasional snow melt (no snow melts in spring). Occurrence in C, D, E climates.
- *Snowmelt-deficit droughts*: caused by a lack of snow-melt discharge in snow-influenced basins in spring due to low precipitation and/or high temperature in winter.
- *Glaciermelt-deficit droughts:* caused by a lack of glaciermelt in summer due to below "normal" temperature during summer.
- *Composite droughts:* caused by several drought generation processes (e.g., multi-year drought).

Hydrological Drought Type	Governing Process(es)	Development	(Lack of) Recovery
Classical rainfall deficit drought	Rainfall deficit (in any season)	*P* control	*P* control
Rain-to-snow-season drought	Rainfall deficit in rain season, drought continues into snow season	*P* control	*T* control
Wet-to-dry-season drought	Rainfall deficit in wet season, drought continues into dry season	*P* control	*P* and *T* control
Cold snow season drought	Low temperature in snow season, leading to:		
Subtype A	Early beginning of snow season	*T* control	*T* control
Subtype B	Delayed snow melt	*T* control	*T* control
Subtype C	No recharge	*T* control	*T* control
Warm snow season drought	High temperature in snow season, leading to:		
Subtype A	Early snow melt	*T* control	*P* control
Subtype B	In combination with rainfall deficit, no recharge	*P* and *T* control	*P* control
Snowmelt drought	Lack of snowmelt in spring due to low *P* or high *T* in winter	*P* and/or *T* control	*P* control
Glaciermelt drought	Lack of glaciermelt in summer due to low *T* in summer	*T* control	*P* or *T* control
Composite drought	Combination of a number of drought events over various seasons	*P* and/or *T* control	*P* control

P, precipitation; *T*, temperature.

Figure 1-4 Drought Propagation Processes (Including Development and Recovery) per Hydrological Drought Type and Subtype (based on Van Loon and Van Lanen85 and Van Loon et al.86)

1.2.2 Catchment control on hydrological process

Catchment control plays a primary role in the drought propagation process. Factors related to the physical catchment structure such as basin area, geology, storage capacity and mean slope significantly influence the hydrological response of the catchment to meteorological drought. The response time of a catchment depends on the hydrological processes occurring in the terrestrial part of the hydrological cycle. These complex processes are dependent on many variables, whose interactions are hardly interpreted. Many publications in literature use different methods to figure out the role of single physical properties of the basins in the terrestrial hydrological process. For hydrological drought development, the most important catchment characteristic is the storage capacity. Major stores in a catchment are snow and glaciers, peat swamps and bogs, the soil column

(particularly when groundwater levels are low), the groundwater system, and lakes and reservoirs. These stores create a long memory in the hydrological system, which determines the transformation of the drought signal (VanLoon et al., 2013). In fact, one of the most important roles is played by the responsiveness of groundwater system. The quickly or slowly responsiveness of groundwater system largely influences hydrograph shape. A fast groundwater response generates flashy hydrographs (short time lag between meteorological and hydrological events), causing more drought events of short duration. On the contrary, a slow groundwater system response generates smooth and lengthened hydrographs with a certain time lag, and hence, longer drought events but attenuated (Van Lanen et al., 2013). Other factors, such as the geology of the catchment (i.e., percentage of hard rock and types of rock), topography, soil (e.g., soil texture and structure), drainage network, land use, and vegetation are dominant in explaining streamflow drought severity (Van Loon, 2013).

In general, through drought propagation process, hydrological drought events are usually less frequent and longer than climatic drought events. Moreover, discharge drought usually reflects the same characteristics of soil moisture drought, in terms of duration and proportion of water deficit. It must be said that, when the response time of the catchment is very fast, hydrological drought characteristics are more like the ones of the meteorological drought in duration and water deficit (Van Loon and Van Lanen, 2012).

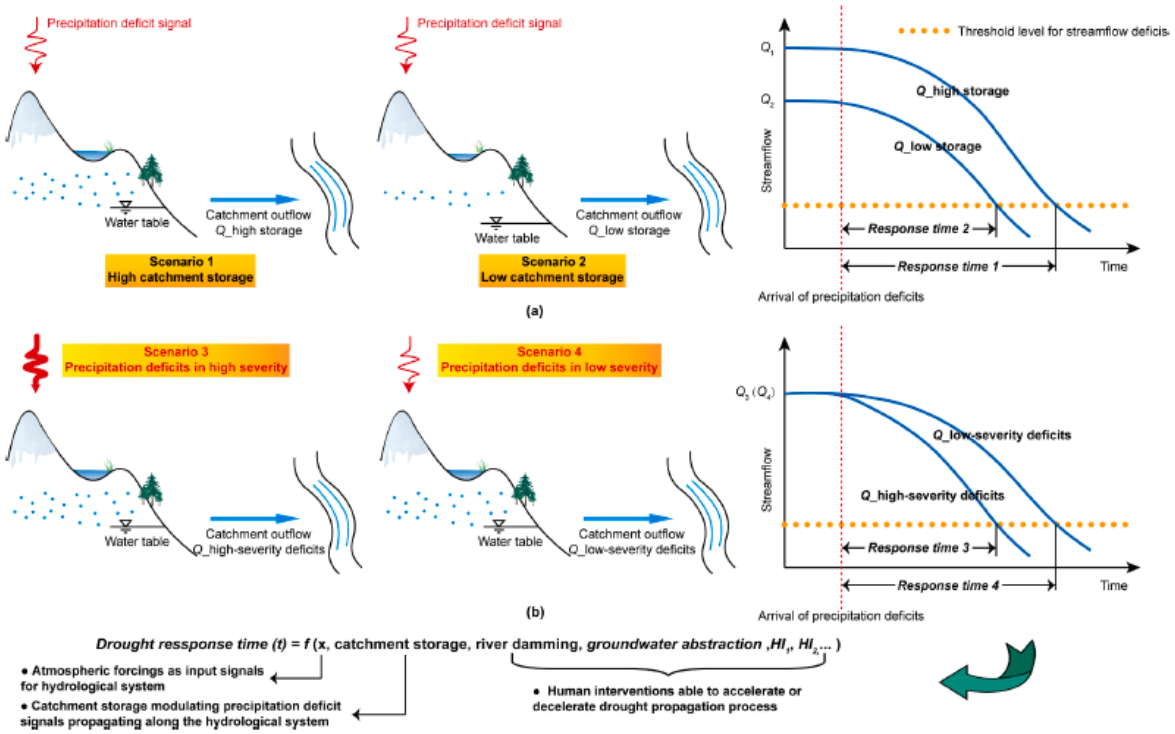

Figure 1-5 A schematic illustrating the control of catchment storage and precipitation deficit severity over drought response time (Fang et al., 2020)

1.3 Drought in Piedmont

After the general analysis of drought phenomenon and its characterization as a "propagation" process, we focus on the assessment of meteorological drought trends since the second half of the last century in Piedmont.

Researching and consulting many studies conducted in Italy about drought trends in the period between the second half of the last century and the first twenty years of the actual century, there is certain evidence that drought periods have increased in frequency and duration in the last 50 years. Nevertheless, a lower number but relevant studies attest a non-significant rise of the trends. An example is given by Haslinger e Blöschl, 2017, who studied temporal series of precipitation in the period 1801-2010 in the Greater Alpine Region. They find out that there is no increase in drought frequency during that period, but only a shift of frequency of drought events from winter-spring seasons (end of XIX century) to autumn (end of XX century) and no

influence of increasing temperature on drought occurrences. Other studies detect an increasing trend in meteorological drought, principally due to increasing temperature which influences potential evapotranspiration. Hanel at al. in 2018 state that the role of rising temperature is increasingly determinant in the drought events of the last years. In agreement with this, Falzoi et al., 2019 do not detect significant trends for SPI in last decades, instead, negative trend in SPEI values during 1981-2017 are visible and are justified by an increase in evapotranspiration rate in time. Similar results were found also by Vogel et al., 2021, who analyse ERA5 dataset by Copernicus Climate Change Service in the years 1979-2018. A third line in the scientific research about drought periods in Italy also detects a variation in precipitation pattern. Specifically, an increase in length of periods of consecutive dry days (not in the frequency), in conjunction with rising SPEI values, is observed by Arpa Piemonte in the study: "Analysis of the regional climate in the period 1981-2010 and trends of the last 60 years" released in 2020. Moreover, it is found that the driest years in the new millennium also involve mountainous areas, while in the last century drought was particularly evident in the lowlands. Pavan et al., 2019, working on meteorological data (1965-2017) of stations located in the North-Centre of Italy, detect a reduction of precipitation (mainly in summer season) in the north-occidental part of Pianura Padana. This is confirmed by Baronetti at al., in 2020, who worked on database SCIA, concluding that "a positive evapotranspiration anomaly seems to have been the main trigger in the period before the 2003, whereas in the last two decades, droughts could be mostly related to precipitation because of changes in their temporal distribution.".

In conclusion it becomes evident that most studies regarding drought in North of Italy and, in particular, in Piedmont, agree in stating that a combination of factors, including temperature and precipitation patterns have changed significantly since the second half of past century, causing an increase in severity and frequency of meteorological drought events.

1.3.1 Most critical drought events in Piedmont

The above-mentioned study by Baronetti et al., 2020 analyses the values of SPI and SPEI indices over the period 1965-2017 in the Po Valley. The study demonstrates how drought is influenced by multiple factors and that the most critical phenomena may have been generated by different meteorological dynamics. The analysis detects the most critical drought events in the Po Valley until 2017, assessing their duration in weeks, the magnitude (sum of SPI and SPEI values/length), and the spatial extent of the phenomenon (Figure 1-6).

	SPEI				SPI		
Period	Length	Magnitude	Area	Period	Length	Magnitude	Area
Nov 23, 1983–Dec 9, 1983	3	−2.6	41	Nov 23, 1983–Dec 9, 1983	3	−3.1	49
Feb 1, 1989–Feb 16, 1989	3	−2.7	29	Jan 23, 1989–Feb 23, 1989	5	−3.4	33
May 16, 1989–Jun 23, 1989	6	−2.5	36	May 23, 1989–Jun 23, 1989	5	−2.9	25
Jul 9, 1990–Nov 23, 1990	19	−2.7	84	Aug 16, 1990–Oct 9, 1990	8	−2.9	51
Nov 16, 1997–Apr 1, 1998	19	−2.8	60	Jan 1, 1998–Apr 1, 1998	13	−4.1	34
Jun 23, 1998–Sep 9, 1998	11	−3.9	66	Aug 1, 1998–Aug 23, 1998	4	−3.5	30
Mar 23, 2002–Apr 23, 2002	5	−2.7	42	Mar 23, 2002–Apr 23, 2002	5	−2.6	51
Aug 16, 2003–Mar 1, 2004	27	−3	58	Oct 9, 2003–Feb 9, 2004	17	−3.7	44
Aug 9, 2007–Oct 16, 2007	10	−2.6	36	Aug 9, 2007–Oct 16, 2007	10	−2.9	33
Mar 9, 2012–Apr 9, 2012	5	−2.4	55	Feb 23, 2012–Apr 9, 2012	7	−3.3	51
Jul 16, 2012–Sep 1, 2012	7	−2.7	48	Jun 1, 2012–Sep 23, 2012	16	−3.3	48
Aug 1, 2017–Dec 23, 2017	20	−3.5	46	Jun 9, 2017–Dec 23, 2017	27	−4.3	51

Figure 1-6 Characterization of extreme drought episodes observed in the 1961–2017 period by SPEI and SPI, calculated at 12 months. For each detected events are reported the propagation gradient, starting week and ending week, and duration length (number of consecutive weeks) Baronetti et al., 2020

Arpa Piemonte published in 2023 a report "Adaptation and Environmental Protection: Piedmont Between Drought and Intense Rainfall", in which, among the other analysis, furnishes a synthetic graph about the most critical drought events in the region, Figure 1-7:

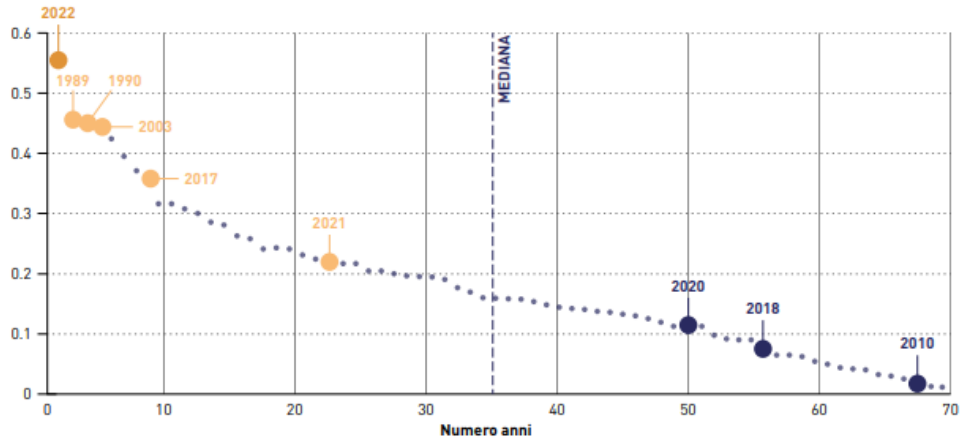

Figure 1-7 Synthetic Drought Classification Index in Piedmont calculated annually from 1950 to 2022. [S2]

To have a clearer idea of the magnitude of the latest drought events occurred in Piedmont, here some info about precipitation and temperature values for three of the "record" events of the new millennium, according to Arpa Piemonte dataset:

- **2003**

  In 2003 it has been registered 728 mm cumulated precipitation with a total of 62 wet days, meaning that there was a deficit of 30% with respect to the mean precipitation in the period 1971-2000. Moreover, summer of 2003 was an extraordinary season with abnormal and very high temperature values. [S3]

- **2017**

  In 2017, Piedmont experienced the third warmest year in the last 60 years, with a temperature anomaly of approximately +1.5°C compared to the climatology of the 1971-2000 period. Additionally, around 700 mm of precipitation fell in Piedmont in 2017, with a rainfall deficit of 351 mm (equivalent to 33%) compared to the 1971-2000 average [S4].

- **2022**

  The year 2022 turned out to be the warmest and the second driest in the entire historical series since 1958. The annual average temperature was approximately 11.4°C, with a positive anomaly of 2.3°C compared to the 1971-2000 period. Cumulative precipitation amounted to 611.9 mm, resulting in a rainfall deficit of 438.6 mm (equivalent to 42%) compared to the climatic average of the three decades from 1971 to 2000. The unprecedented occurrence of such high temperatures and observed drought in the year 2022 redefines the concept of extreme within the historical period considered. [S5]

1.3.2 Future scenarios in Piedmont

Piedmont regional territory is approximately 43% mountainous, and the Alps are a hotspot for climate change, meaning that it is an area where its effects are more evident. It is crucial to understand how the climate has changed in recent years, is expected to change in the future, and what could be the potential impacts on the environment and population. This knowledge represents the base for identifying mitigation and adaptation actions to counteract climate change.

"Over the past 60 years in Piedmont, daily maximum temperatures have shown an increase of 2°C, which has accelerated in the last 35 years; minimum temperatures have risen by approximately 1.5°C.

Precipitation patterns are less regular (with local anomalies in cumulative average annual precipitation), and periods of scarcity are becoming more frequent, alternating with highly concentrated intense rainfall.

In the last 30 years, fresh snow has exhibited a more noticeable negative anomaly at altitudes below 1600-1700 m." (Arpa Piemonte, 2019)

To understand which are the possible future scenarios for Southern Europe related to the changing climate, in this thesis we refer to the Sixth Assessment Report (AR6) of the Intergovernmental Panel on Climate Change (IPCC). Before analysing the possible risks to which Mediterranean area could be subjected, we must identify the different scenarios described by the Representative Concentration Pathways (RCPs) introduced in the Fifth Assessment Report (AR5). Each RCP represents a possible trajectory characterized by the value of the alteration of the energy balance (W/m2) in 2100: RCP2.6, RCP4.5, RCP6.0, RCP8.5. These trajectories depend on the amount of CO2 emissions and pollutant emitted by human activities in the future and are dependent on the mitigation strategies that will be (or not) globally developed and implemented. As far as Southern Europe is concerned, in the AR6 the IPCC identifies four categories of key risks: risk of heatwaves on populations and ecosystems, risks to agricultural production, risks of water resource scarcity, risks arising from increased frequency and intensity of floods. The level of each risk increases with increasing global warming scenario. With low level of climate change adaptation strategies, these risks become more severe with a temperature increase of 2°C compared to a temperature rise of 1.5°C. The risk category concerning "water scarcity" is high, specifically in Southern Europe, where the number of days with insufficient water resources (availability below demand) and drought increases in all scenarios of global warming, affecting respectively, 18% and 54% of the population. Similarly, soil aridity increases with the rise of global warming: in a scenario of a temperature increase of 3°C, soil aridity is 40% higher compared to a scenario with a temperature increase of 1.5°C. [S7] From the AR6, "it is evident that the scientific community, based on the evidence from numerous studies, has reached a certain level of consensus that due to the increase in atmospheric moisture demand and evaporation associated with global warming, the frequency and intensity of drought events are likely to increase in much of Africa, as well as in Australia, Southern Europe, Southern and Western United States, Central America and the Caribbean, North-western China, and parts of South America." (G. Naumann).

In the northern regions of Italy, the prevailing periods of drought are primarily impacted by the North Atlantic Oscillation (NAO) and the Mediterranean Oscillation (MO), linked to the gradient of propagation from North to South (Baronetti et al., 2020). The current dry spell trend, projected also into the twenty-first century, is likely attributed to an intensified positive phase of both NAO and MO, resulting in decreased moisture levels across northern Italy and a significant portion of the Mediterranean basin. In this context northern Italy, which is a crucial region from water resource and European economy point of view, will face "an increase of drought severity, in terms of duration and percentage of drought-affected area, especially for RCP 8.5 and for the later part of the century". Baronetti et al.,2022 say that "the Alpine area (a water tower for the surrounding area) will be significantly affected by higher positive temperature anomalies and increasing drought conditions". In this study it is also reported, for the first time, drought spatial distribution maps of the two meteorological standardized indexes SPI 12 and SPEI 12 for heavy and extreme episodes[3] for the period 2021-2100 and for an increase of 2°C and 3°C scenarios with respect to pre-industrial mean temperature.

[3] Classification of drought episodes in heavy and extreme by means of thresholds. Heavy episodes were defined as those between the index value − 1.65 and − 1.28. Extreme episodes all the drought episodes characterised by an index value < − 1.65.

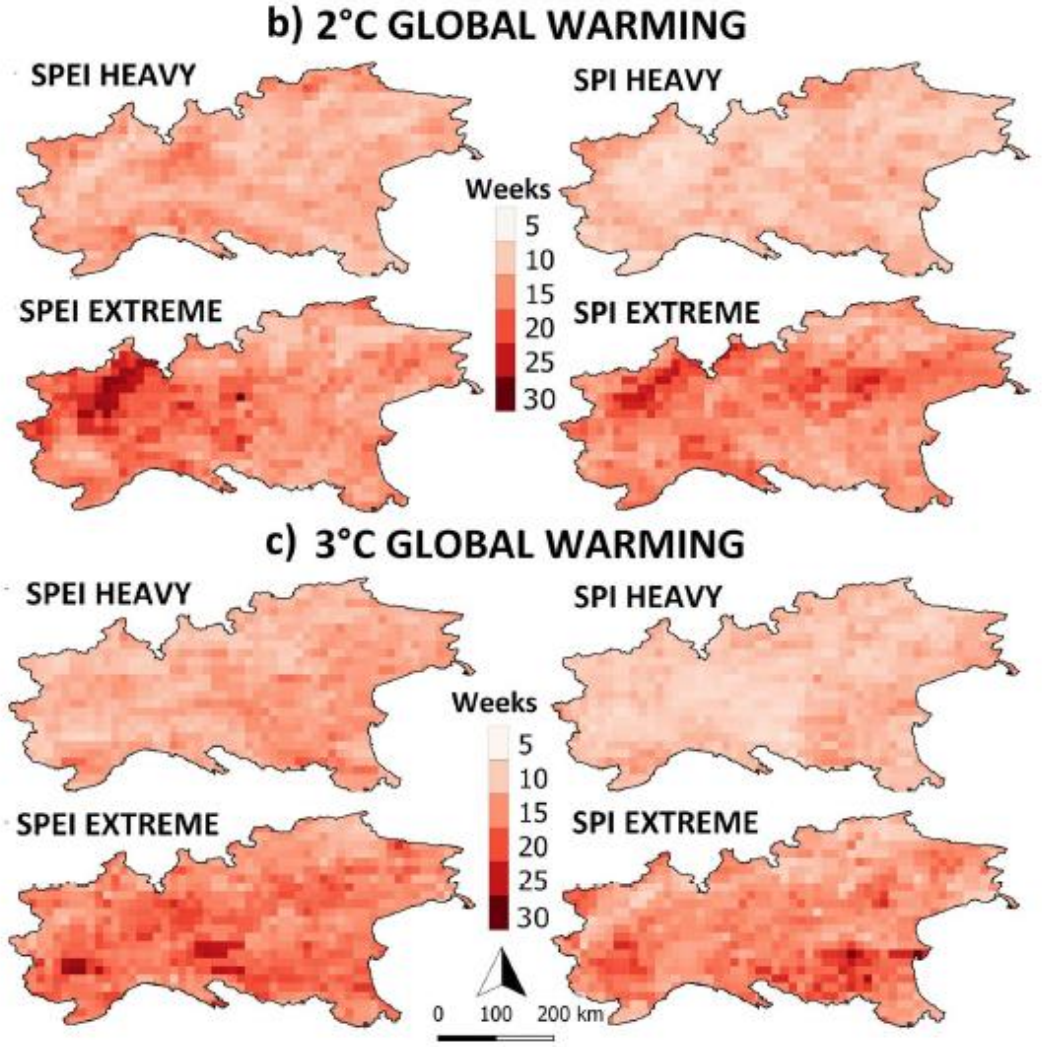

Figure 1-8 Spatial distribution of drought duration (in consecutive weeks) for "heavy" and "extreme" events, computed from SPI and SPEI: b global warming of + 2 °C; c global warming of + 3 °C (Baronetti et al., 2022)

Both SPI and SPEI values output similar results for a global temperature rise of +2 °C: prolonged periods of severe drought will be prevalent in the study area, lasting from 5 to 15 consecutive weeks. In the north-east sectors along the Alps, it is evidenced the occurrence of extreme drought events lasting 20 weeks (Figure 8b). Instead, in the scenario of a +3 °C mean global temperature increase, both for SPI and SPEI it is not detected a substantial amplification of heavy drought events. Extreme drought events, conversely, show higher values of drought duration events. Specifically, the southern part of the Po Plain (comprehending southern Piedmont) is projected to face up to 30 consecutive weeks of drought duration events (Figure 8c). The output shows very clearly the contrast in climate change impacts between +2 and +3 °C. (Baronetti at al., 2022)

2. Study area

Before explaining the methodology and analysing in detail the steps that led to the results of the work, it is useful to frame the study area from a climatic and morphological point of view. Although the study area encompasses only southern Piedmont, there is strong climatic variability within it, mainly due to its morphological heterogeneity that includes the Alpine arc, the pre-Alpine zone, and the Po Valley. In addition, since the quantitative study of meteorological and hydrological drought is conducted on a basin scale, in the second section we focus on the subdivision of the three hydrological basins and their hydro-morphological characterization.

2.1 Climatic characterization of the study area

The southern Piedmont is characterized by a heterogeneous and morphologically complex landscape, mainly related to the difference in elevations between the Alpine arc to the west and the Po Valley. This determines the strong climatic variability within the study area, which significantly influences the hydrological cycle and seasonal processes, foremost among them, for example, the cycle of snow formation and its melting in the spring period. In order to get a clearer idea of the types of climate that characterize southern Piedmont, bibliographic texts were consulted, and finally, the most widely used and internationally recognized climate classification issued in 1936 by Köppen and Geiger is given.

Before focusing on Piedmont climatic classification, we report a brief and general framework of Italian meteorological patterns.

Italy is characterized by diverse climatic conditions. This is because Italy spans from a latitude of 36°N to 47°N, covering a significant portion of the Mediterranean. Moreover, the intricate orography, shaped by the Apennines and Alps, adds complexity to climatic variability. These mountain ranges impact weather fronts and interact with prevailing winds, creating distinct circulation patterns in various regions of Italy. The Alps shield the Po Plain and Venetian Plain from chilly northern currents, while the Apennines, stretching across the peninsula, restrict the influence of moist westerly air to the Tyrrhenian side. Consequently, the Tyrrhenian side is shielded from the cold easterly winds that affect the Adriatic side during the winter season. The moderating influence of the Mediterranean Sea disrupts the air masses flowing through, encouraging the development of depressurizing systems (cyclogenesis) in proximity to the Italian peninsula. The distribution of atmospheric pressure across the Peninsula and surrounding seas (Adriatic, Ligurian, Tyrrhenian, Ionian seas) during different seasons represents a fundamental factor influencing the trends and patterns of meteorological elements. (Fratianni and Acquaotta, 2017). Cantù proposed in 1977 a classification of Italian climatic regions, as shown in Figure 2-1:

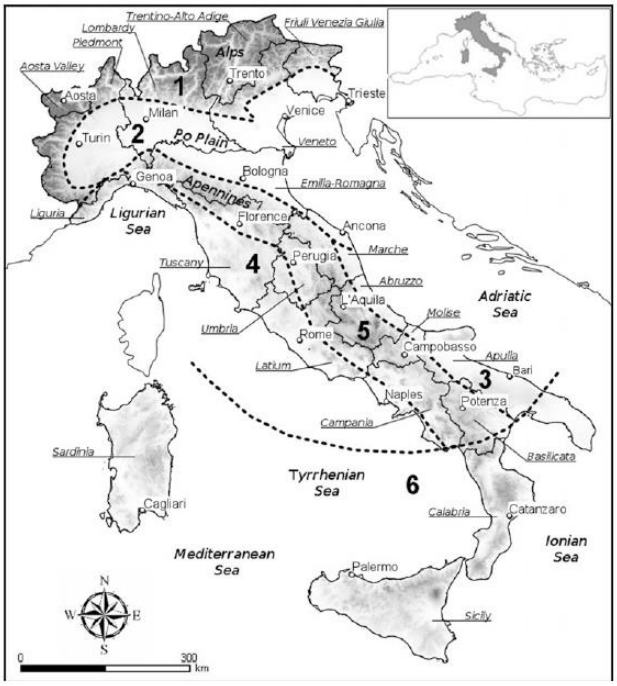

Figure 2-1 The climatic regions of Italy: (1) Alpine Region, (2) Po Plain and Upper Adriatic Region, (3) Central-Southern Adriatic Region, (4) Ligurian and Tyrrhenian Region, (5) Apennine Region, (6) Mediterranean Region (scheme proposed by Cantù 1977, redrawn by D. Garzena)

As we can see, Piedmont comprehends both Alpine region and Po Plain region, which are defined by Cantù in the following way:

- **Alpine region:** It is situated above 1000 m a.s.l. and, during fall, winter, and spring, experiences the influence of various low-pressure systems originating from the Atlantic, the Gulf of Genoa, and the Mediterranean Sea. The climate in the Alpine region is influenced by its elevation, categorized as a cold temperate type that transitions to a nival type at altitudes exceeding 2700–2800 m. The Alps and the pre-Alps receive substantial rainfall, reaching up to 3000 mm annually in areas more exposed to cold air masses from the Pole and warm air from Africa.
- **Po Plain region:** Considering the topography, this climatic region is delineated by the 1000 m contour line on the Alpine side and the watershed line on the Apennine side. Throughout winter, the entire region is enveloped in a layer of cold and stagnant air extending several thousand meters thick. The distinctive characteristic of this climate zone is its pronounced seasonal variation, with summer maximum temperatures often surpassing 30 °C and winter minimums frequently dropping below zero. Rainfall is relatively modest, ranging between 600 and 800 mm annually, with a higher frequency in autumn and spring. Summer also witnesses relatively frequent occurrences of stormy events. (Fratianni and Acquaotta, 2017)

The most famous and used climate classification is the one developed by Köppen and Geiger (1936), that is based on the distribution of mean annual and monthly temperature and rainfall and defines six main climate groups in the world. Italy is located entirely in the Mediterranean climate area and specifically, it is part of the sub-tropical climates with dry summer. According to this classification, the six main groups are represented by a letter: A (tropical), B (arid), C (temperate), D (continental), E (polar) and H (cold due to altitude). A second letter classifies the climate based on the seasonal precipitation and a third indicates the level of heat. A focus on Italy is shown in Figure 2-2:

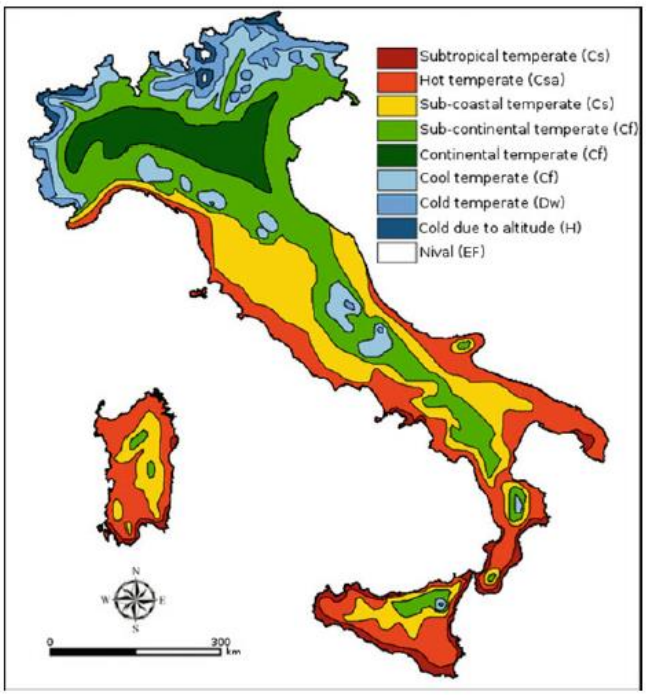

Figure 2-2 Map of climatic classification by Köppen and Geiger (after Pinna 1978, redrawn by D. Garzena)

According to this classification the climates typical of Piedmont region are:

- **Sub-continental Temperate (Cf):** Found in parts of the Venetian Plain, Friulian Plain, coastal Upper Adriatic, and internal peninsular regions. Mean annual temperature ranges from 10 to 14 °C, with the mean temperature of the coldest month varying from -1 to 3.9 °C. Two months experience temperatures exceeding 20 °C, and the annual temperature falls between 16 and 19 °C.
- **Continental Temperate (Cf):** Predominant in the Po Plain and part of the Venetian Plain. Mean annual temperature spans from 9.5 to 25 °C, with the mean temperature of the coldest month ranging from -1.5 to 3 °C. Three months see a mean temperature surpassing 20 °C, and the mean annual temperature exceeds 19 °C. Two sub-types within this category are the hot summer temperate climate (Cfa) and lukewarm summer temperate climate (Cfb).
- **Pre-Alpine and Middle Apennine Region - Cool Temperate (Cf):** Affecting the pre-Alps and the axial zone of the Apennines, sometimes displaying sub-continental characteristics. The mean annual temperature ranges from 6 to 9.9 °C, the mean temperature of the coldest month from 0 to -3 °C, and the mean temperature of the hottest month from 15 to 19.9 °C. The annual temperature is within the range of 18 to 20 °C.
- **Alpine and Upper Apennine Region - Cold Temperate (Dw):** Influencing the Alps and summit areas of higher Apennine groups. Mean annual temperature ranges from 3 to 5.9 °C, with the mean temperature of the coldest month above -3 °C. The mean temperature of the hottest month falls between 10 and 14.9 °C, and the annual temperature is within 16 to 19 °C.
- **Cold due to elevation (H):** impacting the upper sectors of the Alps and the summits of the higher Apennine ranges. (Fratianni and Acquaotta, 2017)

Southern Piedmont is mainly characterized by Cold Temperate (Dw) climate at high altitudes, Cool Temparate (Cf) in the pre-Alps areas, and Sub-continental Temperate (Cf) in the Po Plain area.

In the following paragraph we focus on the hydro-morphological structure of the three basins selected for this study.

2.2 Morphologic characterization of the selected catchments

Currently, in Italy water management is ruled by various legislations, all included in the Part 152/2006 (Environmental Code). Specifically, it comprehends the Water Framework Directive (WFD) 2000/60/EC and Directive 2006/118/EC concerning the protection of groundwater against pollution and deterioration. Moreover, after the enactment of Legislative Decree 152/99 and the WFD, the legislation framework on sustainable water management has been modified. The regulation provides for the division of regional territory into "river basins", within which the land use and water conditions are supervised by the "River Basin Authority".

The hydrographic basin represents the portion of territory that collects surface waters flowing along the slopes and channels them into the same watercourse. The ridgeline of the elevations surrounding the basin is called watershed and separates one basin from another. It is the fundamental physiographic unit to which reference is made in the study of river phenomena and the geomorphological processes related to them. The hydrographic basin of the Po River is the largest in Italy both in terms of length of the main course (650 km) and in terms of area: 86.859 Km². It involves the territories of Liguria, Piedmont, Valle d'Aosta, Emilia-Romagna, Tuscany, Lombardy, Autonomous Province of Trento, Marche, Veneto, also extending to portions of French and Swiss territory. For the Italian portion of the hydrographic basin, the mountainous area accounts for 58%, while the plain area amounts to 42%. (Figure 2-3) [S8]

In the Figure 2-4 the Po basin is subdivided in sub-basins, all related to its direct tributaries. A sub-basin is defined as the portion of territory that collects surface water into the same watercourse of higher order.

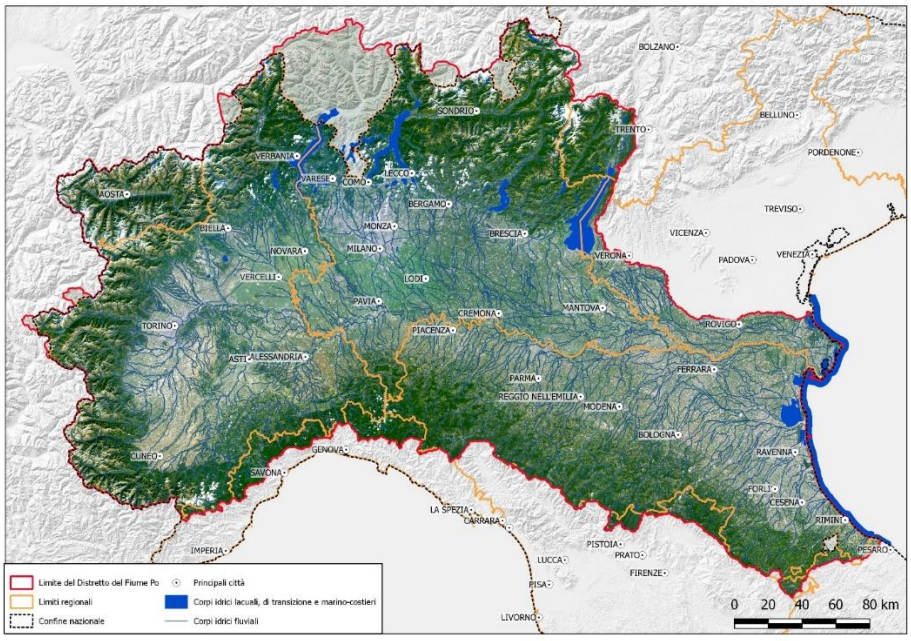

Figure 2-3 Po basin [S8]

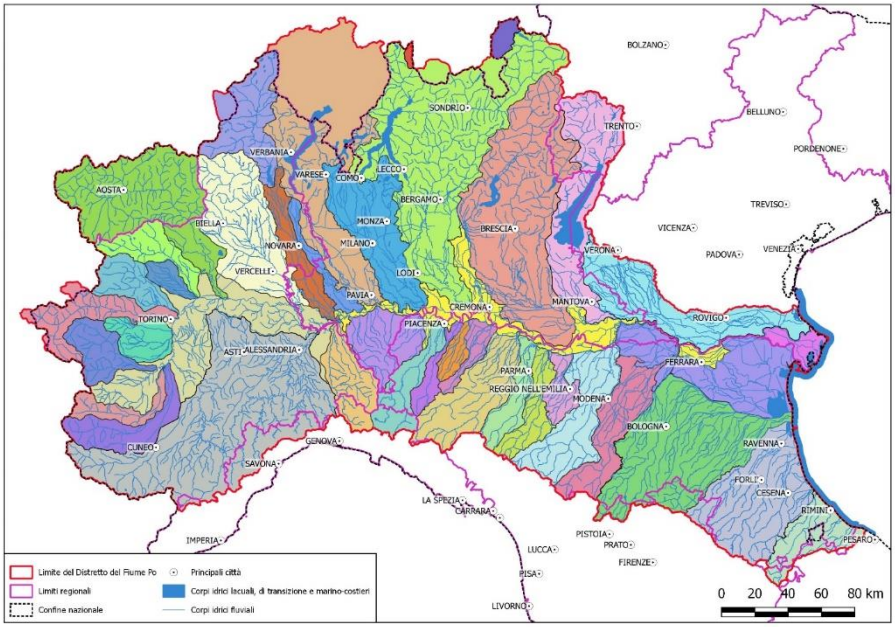

Figure 2-4 Sub-basins of Po basin [S8]

Figure 2-5 Zoom on sub-basins of Piedmont Region [S9]

2.2.1 Varaita basin

The Varaita River basin has an overall area of approximately 600 km2 (1% of the Po River basin), of which 74% is in the mountainous area. The Varaita River (85 km) originates from the two branches of Varaita di Bellino and Varaita di Chianale; the first originates from Mount Maniglia (3,177 m a.s.l.), while the second from the western slope of Monviso. The Val Varaita flows west-east and ends in the Cuneo plain at Costigliole Saluzzo. The main course of the Varaita can be subdivided into two distinct sections based on morphological, morphometric, and hydraulic characteristics: the mountainous section, up to Sant'Antonio, which extends for about half of its course, approximately 42 km, and the plain section up to the confluence with the Po for an additional 42 km [S10]. Maximum altitude: 3848 m a.s.l; Minimum altitude: 237 m a.s.l; Mean slope: 32.3 %. [S18]

Two reservoirs are present in the municipalities of Pontechianale (with a contributing basin area of 67.5 km²) and Sampeyre (with a contributing basin area of 246 km²).

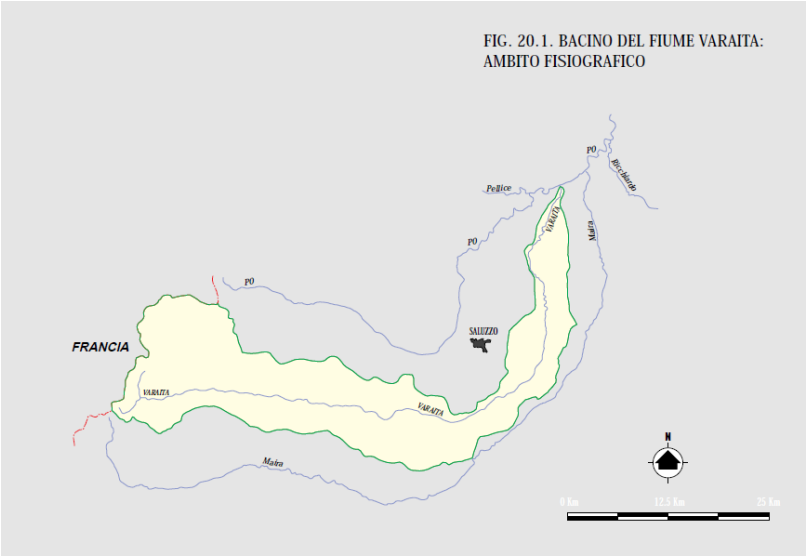

Figure 2-6 Varaita basin

2.2.2 Maira basin

The Maira River basin has an overall area of approximately 1,210 km2 (2% of the Po River basin), of which 59% is in the mountainous area. The Maira River (108 km) starts near Aiguille de Chambeyron (3,471 m a.s.l.) and, following a deeply entrenched and winding valley to Cartignano, flows into the Cuneo plain; near Casalgrasso, it makes a wide turn to the north before merging into the Po. The main course of the Maira can be subdivided into distinct sections based on morphological, morphometric, and hydraulic characteristics: the mountainous section, up to Tetti, which extends for about 41 km, and the plain section up to the confluence with the Po, covering 64 km. [S11]

Maximum altitude: 3310 m a.s.l; Minimum altitude: 231 m a.s.l; Mean slope: 27.9 %. [S19]

Three reservoirs are present: Di Saretto (with a contributing sub-basin area of 52 km²), Di Combamala (with a contributing sub-basin area of 10 km²), and S. Damiano (with a contributing sub-basin area of 450 km²). The first is located in the municipality of Acceglio, while the latter two are situated in the municipality of S. Damiano Macra.

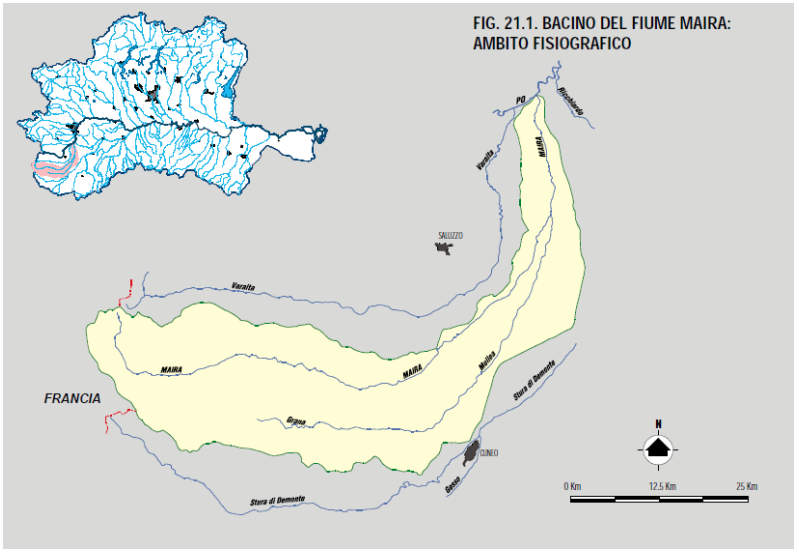

Figure 2-7 Maira basin

2.2.3 Tanaro basin

The Tanaro River basin has an overall area of approximately 8,080 km2 (12% of the Po River basin), of which 82% is in the mountainous area. The plain area is predominantly located in the northeast sector at the confluence with the Po and in the southwest sector corresponding to the plain stretch of the Stura di Demonte. The main branch of the Tanaro River can be subdivided into three distinct sections based on morphological, morphometric, and hydraulic characteristics. The linear development of the riverbed of the Stura di Demonte stream and the mountainous section extends from the source to the confluence with the Corsaglia River (upper Tanaro). The middle section (middle Tanaro) spans from Corsaglia to Castello d'Annone, and finally, the terminal section (lower Tanaro) extends to the confluence with the Po River.

The Tanaro River (276 km) originates at the confluence of Tanarello and the Negrone stream at 2.651 m s.m., in the Alpi Marittime, flows into the high Po Valley at Lesegno, and crosses it with a predominant southwest-northeast direction until it joins the Po near Bassignana. It takes on riverine characteristics with frequent meanders (starting from Farigliano, with a very slow evolution), receiving the Stura di Demonte on the left and skirting the western edge of the Langhe monocline fold on the right, reaching Cherasco. Between Asti and Alessandria, the Belbo stream converges, and downstream of the latter city, the Bormida River, whose main tributary is the Orba.

Maximum altitude: 3197 m a.s.l; Minimum altitude: 76 m a.s.l; Mean slope: 11.54 %. [S20]

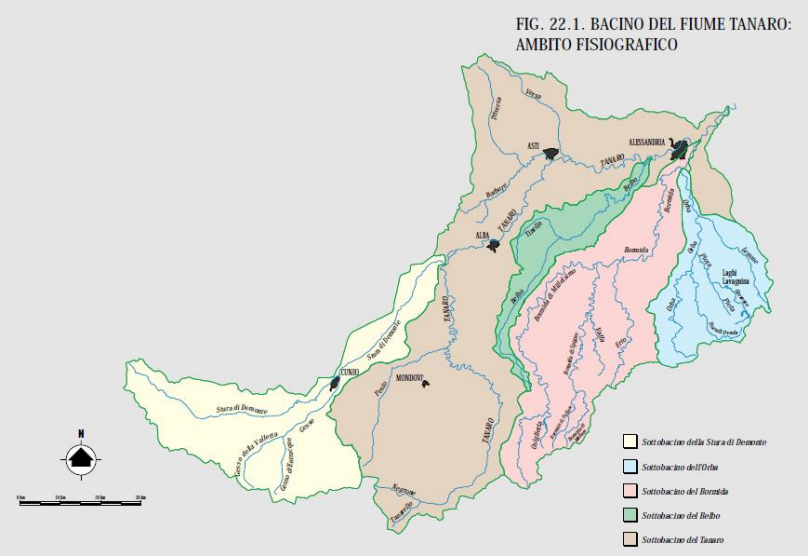

Figure 2-8 Tanaro basin

3. Methodology

Up to this point, we have characterized drought as a complex and multispectral phenomenon, contextualizing it at the local level in the Piedmont region and identifying the most critical events of the last twenty years. We have conducted a brief analysis of potential future scenarios based on different Representative Concentration Pathway (RCP) scenarios and the resulting increase in global average temperature. Subsequently, we have outlined the climate of the Piedmont region, followed by a focus on the morphology of the hydrographic basins under study in southern Piedmont.

The current chapter is focused on the methodology employed to calculate the severity of drought events in the study area. Initially, meteorological, and hydrological droughts are analysed as distinct and independent phenomena through the computation of the Standardized Precipitation Evapotranspiration Index (SPEI) and Standardized Streamflow Index (SSI). Subsequently, the linear correlation coefficient between the two indices is calculated to examine potential correlations.

3.1 Standardized Precipitation Evapotranspiration Index (SPEI)

3.1.1 Introduction

The Standardized Precipitation-Evapotranspiration Index (SPEI) (Vicente-Serrano et al., 2010a; Beguería et al., 2014) is a comprehensive drought indicator that considers both atmospheric evaporative demand and precipitation to assess the intensity and magnitude of droughts across various temporal and spatial scales (ranging from individual stations to global extents). Considering the increase in global temperature, the role of evapotranspiration has become over time more and more decisive in the soil water balance and thus increasingly incisive in drought events. As seen in Chapter 1, in the section on the study of drought in Piedmont, increased evapotranspiration can often be the major cause of a drought event or can however be a relevant contributing factor. This has led researchers to the development of indices that consider both precipitation and evaporative demand of the atmosphere in the computation of drought severity.

An example of one of the most cited and relevant drought indexes that included also evaporation rate is the Palmer drought severity index (PDSI) (Palmer, 1965). The PDSI represents one most important achievement in drought assessment, as it is based on the water balance equation, and therefore it comprehends precipitation, moisture supply, runoff, and evaporation at the surface level. Even if it is considered one of the most complete drought indexes in terms of included hydroclimatic variables, it is strongly influenced by calibration period (fixed temporal scale between 9 and 12 months) and it shows deficiency in spatial comparability, as it is limited to the areas used for its calibration. To overcome the limited spatial comparability, the self-calibrated PDSI has been developed, but it does not fix the temporal problem and it still shows a relevant influence of conditions up to four years in the past on the index values (Guttam, 1998).

Drought indexes must be related to multiple and specific time scales to understand the period of the accumulation deficit. In fact, the time frame between the water input and the availability of water source can vary a lot according to multiple factors. This time lag is due to the hydrological response of the catchment to water input and make the time scale factor essential for managing water resources. For this reason, one of the most used and cited in literature drought indexes is the Standardized Precipitation Index (SPI) developed by McKee et al. in 1993. This index relies only on “standardized precipitation”, which is the "difference of precipitation from the mean over a certain period of time divided by the standard deviation, where the mean and standard deviation are determined from previous data" (McKee et al. 1993). In the development of this index the authors make two fundamental assumptions: 1) the variability of precipitation is much higher than that of other variables, such as temperature and potential evapotranspiration (PET), and 2) the other variables are stationary (i.e., they have no temporal trend). These assumptions make the other hydroclimatic variables negligible and drought events only dependent on precipitation (Vicente-Serrano et al., 2010a). Several authors

find this assumption too unrealistic, principally in relation to increasing global warming during the last century and to projections of growing temperature expected for twenty-first century. Such conditions will lead to dramatic consequences in terms of water demand caused by a higher rate of evapotranspiration. (Sheffield and Wood 2008).

The Standardized Precipitation Evapotranspiration Index (SPEI) combines the characteristics of the PDSI and SPI that have made them largely diffused. In other words, it reintegrates the temperature in drought analysis (as PDSI), but it stands in continuity with SPI computation methodology maintaining its operative features. In fact, the computation process involves generating high-quality Potential Evapotranspiration (PET) data and determining the difference between precipitation and PET (Precipitation – PET) over different time spans (1–48 months as aggregation periods). The differences are then transformed into a standard normal distribution through a log-logistic probability distribution fit, ensuring comparable values across different periods and regions. We must dwell on the concept of Potential Evapotranspiration (PET or ET_0) before continuing with the computation methodology of the index. The term potential evapotranspiration was introduced by Thornthwaite (1948) in the context of the classification of climate: "There is a distinction, then, between the amount of water that actually transpires and evaporates and that which would transpire and evaporate if it were available. When water supply increases, as in a desert irrigation project, evapotranspiration rises to a maximum that depends only on the climate. This we may call "potential evapotranspiration"". So, when we use the term PET, we refer to the maximum amount of water that can evaporate (from bare soil) or transpire (from vegetation) if the supply of water were unlimited (climate as the only controlling factor in evapotranspiration process).

3.1.2 Methodology

In order to obtain the value of SPEI, it is necessary to have available cumulative values of precipitation (generally monthly) and monthly cumulative values of ET_0. In our study, the first variable is computed by summing the daily precipitation value for each month, obtaining monthly precipitation timeseries. The latter can be calculated using various formulas, which require different input data. ET_0 equation types can be temperature-based, radiation-based, and combination equations (Figure 3-1, McMahon, 2013). In order of complexity, these models are the Thornthwaite (Thornthwaite,1948), Hargreaves (Hargreaves & Samani, 1985), Penman-Montieth with Hargreaves radiation term referred to here as P-M (Hargreaves) (Allen et al., 1998), Priestley-Taylor (Priestley &Taylor, 1972), and FAO-56 Penman-Montieth referred to here as P -M (FAO-56) (Allen et al.,1998). The FAO-56 reference crop definition (Allen et al., 1998) is used for all ET_0 models except for the Thornthwaite equation, which uses the original Thornthwaite (1948) definition.

PET Groups	Group 1 Empirical	Group 2 Temp-Proxy Radiation		Group 3 Observed Radiation	
PET Model	Thornthwaite	Hargreaves	P-M (Hargreaves)	Priestley- Taylor	P-M (FAO56)
Mean temp	X	X	X	X	X
Min/Max temp		X	X		
Wind speed			X		X
Surface pressure					X
Specific humidity					X
Radiation	T_{mean}	T_{max}–T_{min}	T_{max}–T_{min}	WFD	WFD
Reference	Thornthwaite (1948)	Hargreaves-Samani (1985)	Allen *et al.* (1998)	Priestley-Taylor (1972)	Allen *et al.* (1998)

Figure 3-1 PET models (McMahon, 2013)

Of these, the Hargreaves formula (Hargreaves et al., 1986) was chosen, in the absence of the data needed to calculate other formulas such as FAO-56 Penman-Monteith. Three quantities are needed for the purpose of calculation: site latitude, mean maximum temperature, and mean minimum temperature. The latitude is needed to calculate the extra-terrestrial solar radiation $\left(\frac{\text{MJ}}{\text{m2 day}}\right)$ according to the formula:

$$R_a = \frac{24 \cdot 60}{\pi} \cdot G_s\, d_r \left(\omega_s\ sen(\varphi)\, sen(\delta) + \cos(\varphi)\cos(\delta)\ sen(\omega_s)\right)$$

Where:

- $\boldsymbol{G_s}$: $Solar\ costant\ \left(\frac{\mathrm{MJ}}{\mathrm{m2\ min}}\right)$; $G_s = 0{,}0820$;
- $\boldsymbol{\varphi}$: $Latitude\ (rad)$;
- $\boldsymbol{d_r}$: $Inverse\ of\ the\ distance\ Earth - Sun$; $d_r = 1 + 0{,}033 * \cos\left(\frac{2\pi J}{365}\right)$;
- $\boldsymbol{\delta}$: $Solar\ declination\ (rad)$; $\delta = 0{,}4093 * sen\left(\frac{2\pi J}{365} - 1{,}405\right)$;
- $\boldsymbol{\omega_s}$: $Solar\ angle\ at\ sunset\ (rad)$; $\omega_s = \arccos(-tan\varphi\ tan\delta)$;
- J: $Julian\ day\ (day)$;

Once obtained the value of the extra-terrestrial solar radiation, we can compute the potential evapotranspiration ET_0 (mm) with the Hargreaves formula:

$$ET_0 = 0.0023 \cdot 0.408(T_{mean} + 17.8)(T_{max} - T_{min})^{0.5} R_a$$

In this formula T_{mean}, T_{max} and T_{min} represent the monthly means of the daily mean, maximum and minimum temperature. Instead, 0.0023 is an empirical value and 0.408 converts the extra-terrestrial radiation in mm/day.

We can now compute the difference D_i (mm) between monthly precipitation P_i and monthly potential evapotranspiration ET_{0i} as:

$$D_i = P_i - ET_{0i}$$

which provides a simple measure of the water surplus or deficit for the analysed month *i*.

While for SPI a two-parameter distribution shows a good fit for all the series (usually gamma distribution), for SPEI series we must consider that the value D_i can assume negative values. Therefore, three-parameter distributions have been selected by Vicente-Serrano in 2010 to fit the D_i values. Using empirical L-moment ratio in order to fit the probability distributions to the samples of data, they found out that more distribution adjusted very well to the empirical probabilities. So, they based their selection on the extreme values (low ones) adaptability of the distributions, selecting the log-logistic distribution (Vicente-Serrano, 2010a), expressed as:

$$f(x) = \frac{\beta}{\alpha}\left(\frac{x-\gamma}{a}\right)^{\beta-1}\left[1 + \left(\frac{x-\gamma}{a}\right)^{\beta}\right]^{-2}$$

Where α, β and γ are the three parameters of the distribution and represent respectively scale, shape, and origin parameters, for D_i values in the range $\gamma > D_i < \infty$.

In order to fit the log-logistic distribution, it is first necessary to calculate the probability weighted moments (Probability weighted moments or PWM in the literature) by the unbiased method of Hosking (1986). Given an increasing ordered set of data, the moment *w* of order *s* is equal to:

$$w_s = \frac{1}{N}\sum_{i=1}^{N} \frac{\binom{N-i}{s} D_i}{\binom{N-1}{s}}$$

Where *N* is the total number of the series.

Once computed the PWMs, it is possible to calculate the three parameters of the distribution for each D_i series:

$$\beta = \frac{2w_1 - w_0}{6w_1 - w_0 - 6w_2}$$

$$\alpha = \frac{(w_0 - 2w_1)\beta}{\Gamma(1+\frac{1}{\beta})\Gamma(1-\frac{1}{\beta})}$$

$$\gamma = w_0 - \alpha\Gamma\left(\frac{1+1}{\beta}\right)\Gamma\left(\frac{1-1}{\beta}\right)$$

Where $\Gamma(\beta)$ is the gamma function of β.

Then we can proceed by computing the non-exceedance probability for each value i of each month j. The cumulative probability of $D_{i,j}$, according to the log-logistic distribution, is given by:

$$F(D_{i,j}) = \left[1 + \left(\frac{a_j}{D_{i,j} - \gamma_j}\right)^{\beta_j}\right]^{-1}$$

Once obtained the cumulative probability, the $D_{i,j}$ is normalized by subtracting the mean and dividing by the standard deviation of the series D_j. In this way we obtain a normal distribution with zero mean and a standard deviation equal to one for each monthly series. This method is repeated for the aggregation periods (timescales) of 3, 6, 9, 12 and 24 months, meaning that the mean is computed on a moving window comprehending respectively 3, 6, 9 12, and 24 months including the month D_j for which the probability must be computed.

This method has been implemented on Matlab and already tested for previous research that achieved good and reliable results.

3.1.3 Drought index interpretation

The characterisation of droughts for both SPI and SPEI is based on the SPI scale (Mckee et al., 1993). The SPI scale is used since the computation of both indices is based on the same principles. (Tirivarombo et al., 2018).

According to the "*run theory*" (Yevjevich, 1967), the length of time (months) that the drought index is consecutively at or below a truncation level (usually -1) is the drought duration, and the total duration of the drought is considered one event (Zambreski, 2016). Drought severity (S) is computed as the cumulative sum of the index value based on the duration extent. Meanwhile, the intensity (magnitude) of an event is the severity divided by the duration. Events that have a shorter duration and higher severity will have high drought intensities (Ojara et al., 2022).

Drought classes	SPEI values
Extremely wet (EW)	≥2.0
Severe wet (SW)	1.5 to 1.99
Moderate wet (MW)	1.0 to 1.49
Normal (N)	– 0.99 to 0.99
Moderate dry (MD)	– 1.0 to – 1.49
Severe dry (SD)	– 1.5 to – 1.99
Extreme dry (ED)	≥2.0

Figure 3-2 Categorization of drought and wet grade according to the SPEI (Wang et al., 2014).

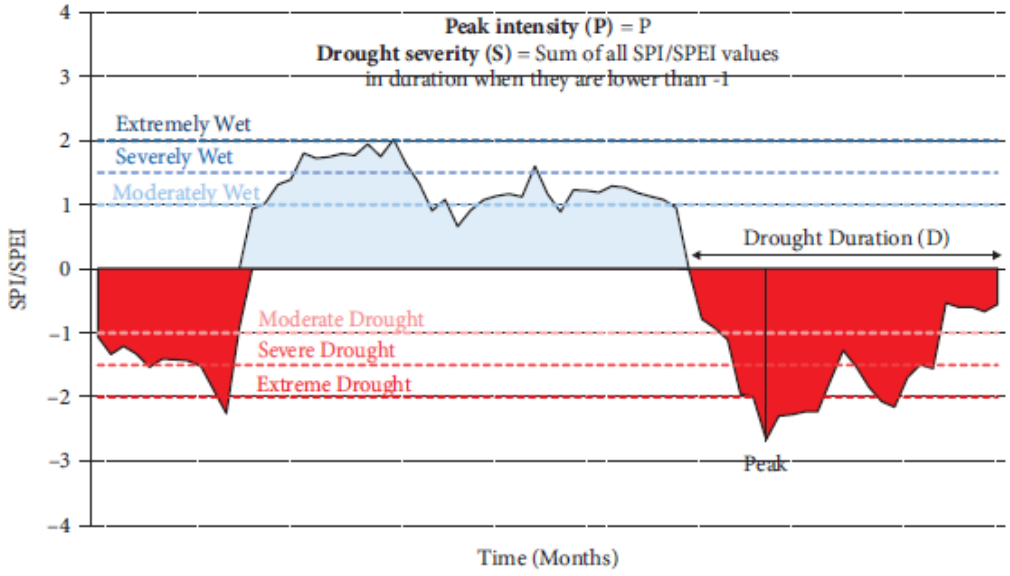

Figure 3-3 Drought characteristics: duration, severity, and intensity (Hakam at al., 2022)

3.2 Standardized Streamflow Index (SSI)

3.2.1 Introduction

The *Standardized Streamflow Index (SSI)* has been developed by Vicente-Serrano et al. in 2012 with the aim of characterizing hydrological drought as an independent phenomenon from meteorological drought. The principle at the base is, in fact, that no direct spatial and temporal relationship exists between the two phenomena (Vicente-Serrano and López-Moreno 2005).

The research on the quantification of indexes that could represent hydrological drought severity has started later than the meteorological drought. Consequently, they are still less used than meteorological drought indexes and the assessment of hydrological droughts is typically reliant on the run theory (Yevjevich 1967). Run theory consider the period of a drought event as the time frame during which values of the hydrological variables are below a certain truncation level, and the severity as the cumulated deviation from the truncation level during that time frame. This method results inefficient for two main reasons: dependence on seasonality and impossible comparison among different basins. For rivers with strong seasonality run theory does not consider that the streamflow values during high-flow season can have impacts on the streamflow values during low-flow periods (months later). This is due to the depletion of reservoirs downstream, which reduces the streamflow during low-flow season (usually summer). Moreover, this method does not allow the comparison between drought periods and the creation of drought maps in adjacent basins, due to the variability in river regimes and flow magnitudes. These are the reasons why, researchers have started indagating the idea of a standardized approach that enables the comparison of drought severity for different climates and regimes. The main issues on the development of a standardized index are related to the number of factors influencing hydrological series, such as topography, lithology, presence of reservoirs and vegetation. All these elements create a high spatial variability in hydrological series and make it difficult to find a probability function that may fit well all monthly streamflow data across extensive regions. In the publication titled "Accurate computation of a streamflow drought index" in 2012, Vicente-Serrano assessed the performance of various probability distributions, considering the possibility that different distributions may be fitting for each month. The aim was to calculate the Standardized Streamflow Index (SSI). This evaluation has facilitated the development of a precise procedure to derive a hydrological drought index, beneficial for conducting spatial and temporal comparisons across diverse river regimes and flow characteristics.

3.2.2 Methodology

To implement the SSI, it is needed the availability of mean monthly streamflow Q_i data. We apply this procedure to the monthly series at the closing sections of the three rivers object of study (Varaita, Maira and Tanaro). Moreover, the following procedure recalls the method developed by Vicente-Serrano et al., (with some modifications explained below).

To compute the drought indexes, two methods can be exploited: the use of a single probability distribution for all the monthly series and for all the catchments, or the use of different probability distributions for the different monthly series, according to their fitting to each single series. In this study we choose to follow the first approach, considering that all the selected distributions show a high goodness-of-fit to the data. Moreover, this method makes the analysis simpler and easily reproducible.

In order to find the probability function that has a good adaptability to our data, we select three probability distribution functions with two parameters: the Log-normal, the Weibull, and the Gamma distributions and two distribution functions with three parameters: the Generalized Extreme Value (GEV) and the Log-logistic distributions. The aim is to find a probability distribution suitable for all the data series.

- *Log-normal distribution*
  The log normal cumulative distribution function (cdf) is expressed as:

$$F(x) = \frac{1}{\sigma\sqrt{2\pi}} \int_0^x \frac{1}{t} exp\left\{\frac{-log(t-\mu)^2}{2\sigma^2}\right\} dt, \quad for \ x > 0$$

  And it is implemented by using the MATLAB `logfit` function that gives the maximum likelihood parameter estimates, that are the mean $\boldsymbol{\mu}$ and standard deviation $\boldsymbol{\sigma}$. To plot the probability distribution, we used the `logncdf` function.

- *Weibull distribution*
  The Weibull cumulative distribution function (cdf) is expressed as:

$$F(x) = 1 - e^{-\left(\frac{x}{a}\right)^b}$$

  And it is implemented by using the MATLAB `wblfit` function that gives the maximum likelihood parameter estimates, that are the scale parameter ***a,*** and the shape parameter ***b***. To plot the probability distribution, we used the `wblcdf` function.

- *Gamma distribution*
  The Gamma cumulative distribution function (cdf) is expressed as:

$$F(x) = \frac{1}{b^a \Gamma(a)} \int_0^x t^{a-1} e^{\frac{-t}{b}} dt$$

  And it is implemented by using the MATLAB `gamfit` function that gives the maximum likelihood parameter estimates, that are the shape parameter ***a,*** and the scale parameter ***b***. To plot the probability distribution, we used the `gamcdf` function.

- *Generalized Extreme Value (GEV) distribution*
  The GEV cumulative probability distribution function (cdf) is expressed as:

$$F(x) = e^{-(1-\frac{k(x-\mu)}{\sigma})^{\frac{1}{k}}}$$

And it is implemented by using the MATLAB `gevfit` function that gives the maximum likelihood parameter estimates. The three parameters are $\boldsymbol{k}$ shape parameter, $\boldsymbol{\sigma}$ scale parameter and $\boldsymbol{\mu}$ location parameter and the `gevcdf` to obtain cumulative probability values.

- *Log-logistic distribution*
  The log-logistic cumulative distribution function (cdf) is expressed as:

$$F(x) = \left[1 + \left(\frac{a}{x-\gamma}\right)^{\beta}\right]^{-1}$$

And it has been implemented on MATLAB computing the Probability Weighted Moments and then the three parameters, using the same procedure explained at chapter 3.1.2.

In order to carry out a first visual analysis of the distributions fitting the data, we plot the five distributions with the empirical distribution function (edf), using the Weibull plotting position given by:

$$F(x_i) = \frac{i}{N+1}$$

Where N represents the total observations of the sample.

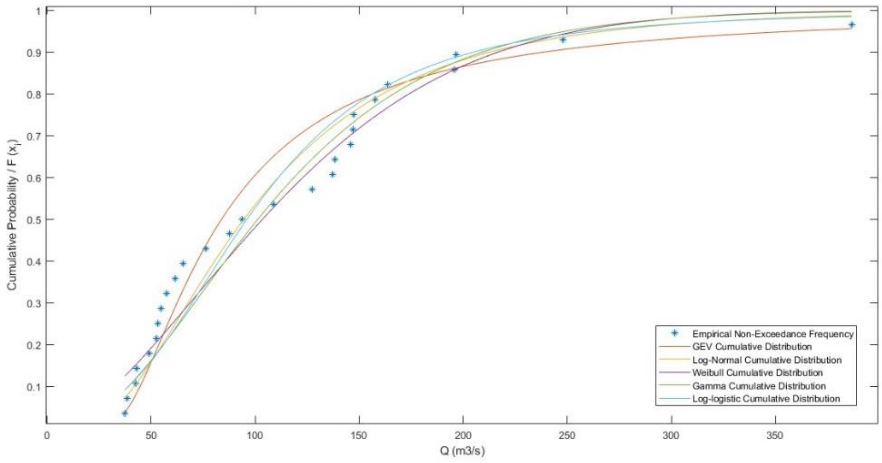

Figure 3-4 CDFs and EDF for monthly streamflow series of January of Tanaro River at Montecastello

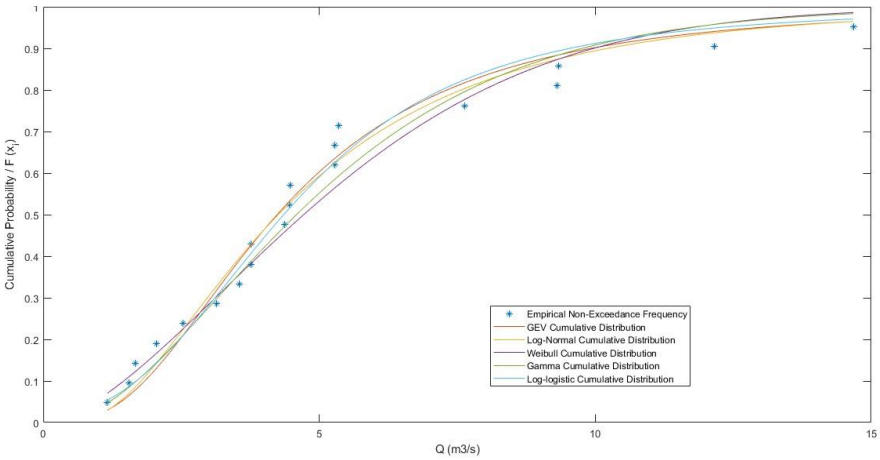

Figure 3-5 CDFs and EDF for monthly streamflow series of March of Varaita River at Palonghera

The capability of these five probability distributions to represent all monthly streamflow data is quantified and tested through goodness-of-fit $Chi-squared\ (\chi^2)$ test and the *Kolmogorov-Smirnov test* both implemented on MATLAB and with a level of significance of 5%. The functions used to apply these tests to all the monthly streamflow series are respectively: the `chi2gof` and `kstest`.

From the $\chi^2\ test$ or Pearson test it is not possible to detect which is the probability distribution that best aligns with the data, as the test does not reject no distribution selected for almost each monthly series of each river considered. An example is given in Figure 3-6:

Chi-squared test results with 5% level of significance

Month	GEV	Log-normal	Weibull	Gamma	Log-logistic
{'January' }	0	0	0	0	0
{'February' }	0	0	0	0	0
{'March' }	0	0	0	0	0
{'April' }	0	0	1	0	0
{'May' }	0	0	0	0	0
{'June' }	0	0	0	0	0
{'July' }	0	0	0	0	0
{'August' }	0	0	0	0	0
{'September'}	0	0	0	0	0
{'October' }	0	0	0	0	0
{'November' }	0	0	0	0	0
{'December' }	0	0	0	0	0

Figure 3-6 Chi-squared test for the Tanaro River monthly streamflow

Figure 3-6 shows the results of the goodness-of-fit given by the chi-squared test for the five distributions applied to streamflow monthly series of Tanaro river. The `chi2gof` function releases the value 0 if the test accepts the null hypothesis (the sample comes from the given distribution), and 1 if it rejects the null hypothesis. As we can see the only monthly distribution rejected is the Log-normal one for April. The test shows a good adaptability of all the distribution also for Varaita and Maira monthly streamflow series.

Therefore, we continue the process of selection of one single distribution that could represent all the data. We apply the Kolmogorov-Smirnov (KS) test suggested by Vicente-Serrano et al., 2012. The test accepts the null hypothesis for all the streamflow series. The p-value is high in all the cases but showing very high values (p-value ranges from 0 to 1) for the Log-logistic distributions (all the p-values > 0.6) for all the series of the three rivers. We then, indagate the KS D statistics values. We obtain twelve values of D (for each monthly series), that represents the maximum distance of the distribution tested from the sample values.

$$D = max\ (|F(x) - G(x)|)$$

Where $F(x)$ is the probability distribution and $G(x)$ the empirical probability distribution.

To understand which probability shows the minimum distance D, we plot the D values of each distribution in boxplots (Figure 3-7).

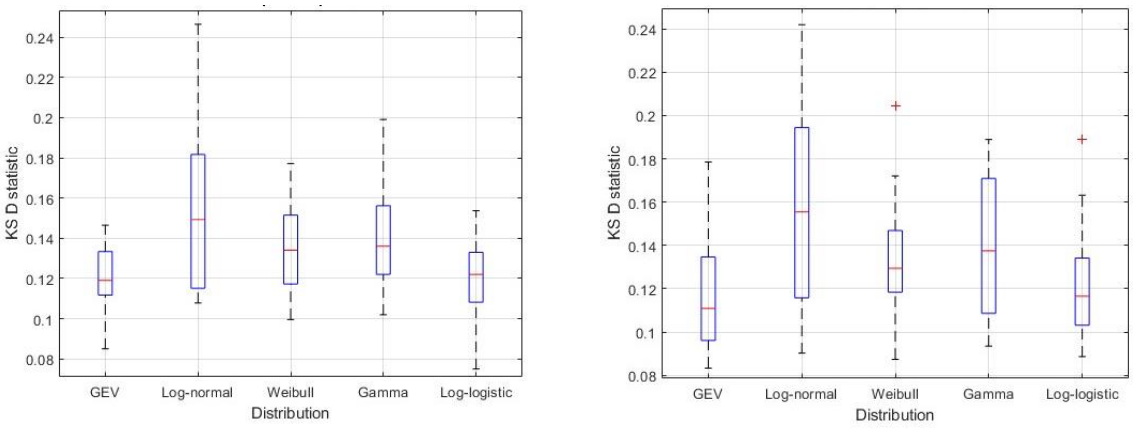

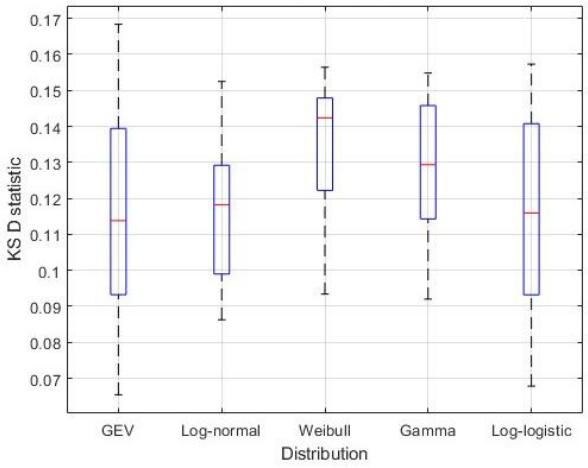

Figure 3-7 KS test, D values of the Varaita (top left), Maira (top right) and Tanaro (bottom) rivers

Given the results of the boxplots, which show good results for all the five distributions, it has been decided to choose the Log-logistic distribution to represent all the data series, because it has a low median for all the river data and a small standard deviation for Maira and Varaita rivers.

The SSI is then obtained as the standardized value of the cumulative log-logistic distribution $F(x_{i,j})$ following the classical approximation of Abramowitz and Stegun (1965):

$$SSI = W - \frac{C_0 + C_1 W + C_2 W^2}{1 + d_1 W + d_2 W^2 + d_3 W^3}$$

Where the constants are C0 =2.515517; C1 = 0.802853; C2 = 0.010328; d1 = 1.432788; d2= 0.189269 and d3= 0.001308. And W is given by:

$$W = \sqrt{-2\ln(P)} \quad \text{for} \quad P \leq 0.5$$

P is the probability of exceeding a determined $x_{i,j}$ value, given by: $P = 1 - F(x_{i,j})$. If $P > 0.5$, then P is replaced by 1-P and the sign of the resultant SSI is reversed (Vicente-Serrano et al., 2012).

3.2.3 Drought Index Interpretation

The SSI is interpreted in literature in the same way as the SPEI and SPI indexes (see paragraph 3.1.3). The only difference in this study is that the SSI is not computed on different time scales (aggregation periods) such as the SPEI, as it considers streamflow data series that already comprehend the aggregation in time and space of the runoff deriving from such precipitation. For this reason, it has been decided to consider the SSI only on a monthly scale.

3.3 Correlation coefficient (Pearson)

The last step of the methodology followed in this study regards the relationship between the Standardized Precipitation Evapotranspiration Index (SPEI) at 1,3,6,9,12 and 24 months and the Standardized Streamflow Index (SSI). Firstly, we conduce a correlation analysis using the linear correlation coefficient for the series of SPEIs and SSI on the whole period. Secondly, we compute the correlation coefficient for the single monthly series, in order to detect if the relationships between SPEIs and SSI are subjected to seasonal variations (Vicente-Serrano et al., 2012). The linear correlation coefficient (Pearson coefficient) has been computed on MATLAB, exploiting the function `corrcoef`.

The equation of the linear correlation coefficient is:

$$\rho\ (A,B) = \frac{1}{N-1}\sum_{i=1}^{N}\left(\frac{A_i-\mu_A}{\sigma_A}\right)\left(\frac{B_i-\mu_B}{\sigma_B}\right)$$

Where N is the total number of observations, μ_A and σ_A are the mean and standard deviation of A, respectively, and μ_B and σ_B are the mean and standard deviation of B. A and B represent the values of the $SPEI_i$ and SSI_i.

4. Data collection and analysis

The present study on drought in southern Piedmont has been implemented by studying meteorological and hydrological drought as independent phenomena. This analysis provides for the computation of the monthly Standardized Precipitation Evapotranspiration Index (SPEI) (1,3,6,9,12 and 24 time scales) to describe meteorological drought and of the monthly Standardized Streamflow Index (SSI) for the assessment of hydrological drought. The development of these two indexes requires the collection respectively of monthly precipitation and evapotranspiration data series and of monthly streamflow data series. The characteristics of the two datasets are discussed below in this preliminary analysis.

4.1 Precipitation and evapotranspiration data

As said in the previous chapter, the drought analysis has been conducted on a basin scale, meaning that for each catchment we must compute single monthly timeseries both for SPEIs and SSI, to, then, examine the relationship between them. The monthly SPEIs development requires precipitation and evapotranspiration timeseries.

4.1.1 Data source

The data analysed come from the NWOI dataset, maintained, and updated by the Arpa Piemonte Forecast Systems Department [S13]. The data grid covers the 6.5-9.5 W and 44.0-46.5 N domain in longitude and latitude, with a resolution of 0.125° and WGS84 projection. The time span of the data is from December 1, 1957, to November 16, 2023. We download three netCDF files containing respectively daily precipitation, daily maximum and minimum temperature in the time span indicated. Areal data are provided as a database with already analysed and validated values. The data used for interpolation were obtained from the network of the Italian "Servizio Idrografico e Mareografico Nazionale" and the telemetry network of Arpa Piemonte; the interpolation method chosen is optimal interpolation, based on minimizing the variance of the analysis error [S15].

In order to study the area on a basin scale we download the shapefiles containing the watersheds of Piedmont catchments. The regional territory is divided into three levels (561 first-level basins, 41 second-level basins and 27 third-level basins). The watersheds were derived from the perimeter with morphological criteria on IGMI 1:25,000 and IGMI 1:100,000 cartography and then, for lowland areas only, on CTR 1:10,000 cartography. The projection is WGS84/UTM 32N. These files are released by Arpa Piemonte and found in Geoportale Piemonte [S14].

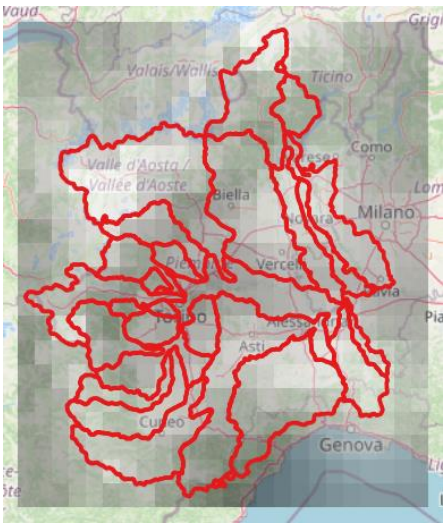

Figure 4-1 Example of third level catchments watersheds shapefile superposed to netCDF file. Scale 1: 3500000 - WGS 84

4.1.2 Data analysis

From the series of daily values provided for each cell in the spatial domain of the netCDF files, the series of monthly precipitation, i.e., sum of daily values for the entire month, and monthly average maximum and minimum temperature, i.e., the average of the maximum and minimum temperature during each month, respectively, are obtained. According to the methodology explained in Chapter 3 we compute the monthly Precipitation (P), monthly Potential Evapotranpriration (PET), and monthly Water Balance (D) and then the monthly SPEIs for the aggregation periods of 1, 3, 6, 9, 12 and 24 months as grid data in netCDF files. These files have the same domain in longitude and latitude, same resolution of 0.125° and WGS84 projection as the original precipitation and temperature files. We, then, work on the netCDF files containing the monthly hydroclimatic variables and SPEIs on QGIS 3.24.

Of the shapefiles provided by Arpa Piemonte, the high-level (third-level) watersheds file is exploited but bringing some changes to the perimeters of the catchments. Specifically, we want to work on basins related to direct tributaries of Po River, as seen in the Chapter 2. The Tanaro River basin in this file is split in the sub-basins of the Stura di Demonte River, the Belbo-Bormida-Olba rivers, and the Tanaro River, as it is shown in Figure 4-2. Using the function "fondi elementi selezionati" we join the three sub-basins in the bigger one related to the Tanaro River with closing section at Alessandria (Figure 4-3).

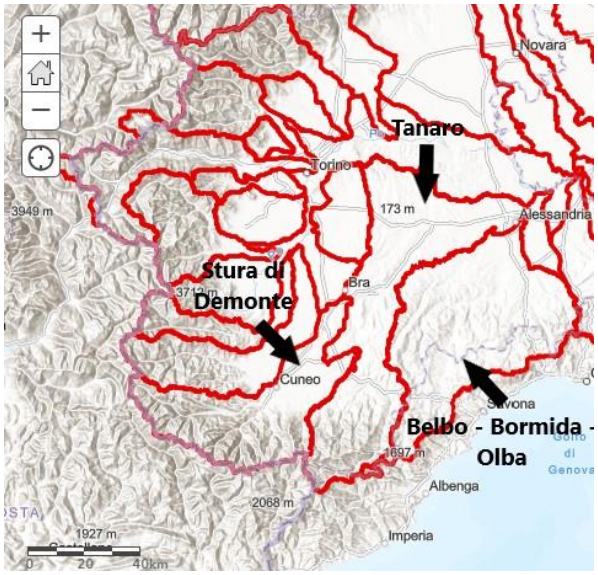

Figure 4-2 Original subdivision (third-level) of the Tanaro basin of Arpa Piemonte shapefile

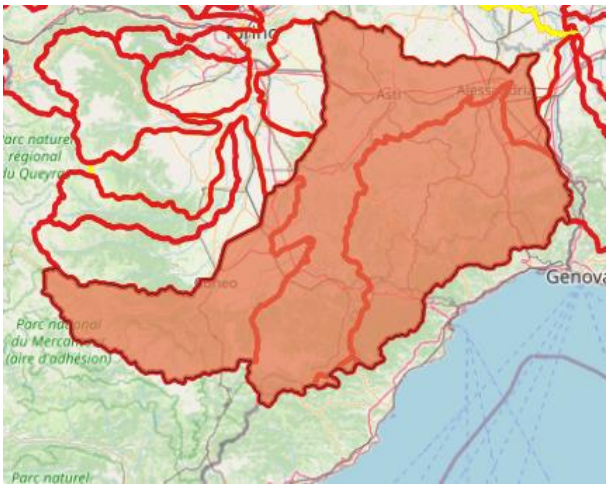

Figure 4-3 Joint of the three original sub-basins in the Tanaro basin with closing section at Montecastello

Obtained the right basins subdivision, the first analysis has been conducted with aim of computing the spatial mean of monthly Precipitation (P), monthly Potential Evapotranspiration (PET), and of the monthly Water Balance at soil level (D) (Chapter 3.1.2) at basin scale. This procedure has been implemented on QGIS, exploiting the function "zonal statistics (multiband)", that allows to compute the spatial mean of the three variables on each catchment for each month of the time span December 1957 – October 2023. (Example of P, PET and D spatial distribution in January 2020, Figure 4-4)

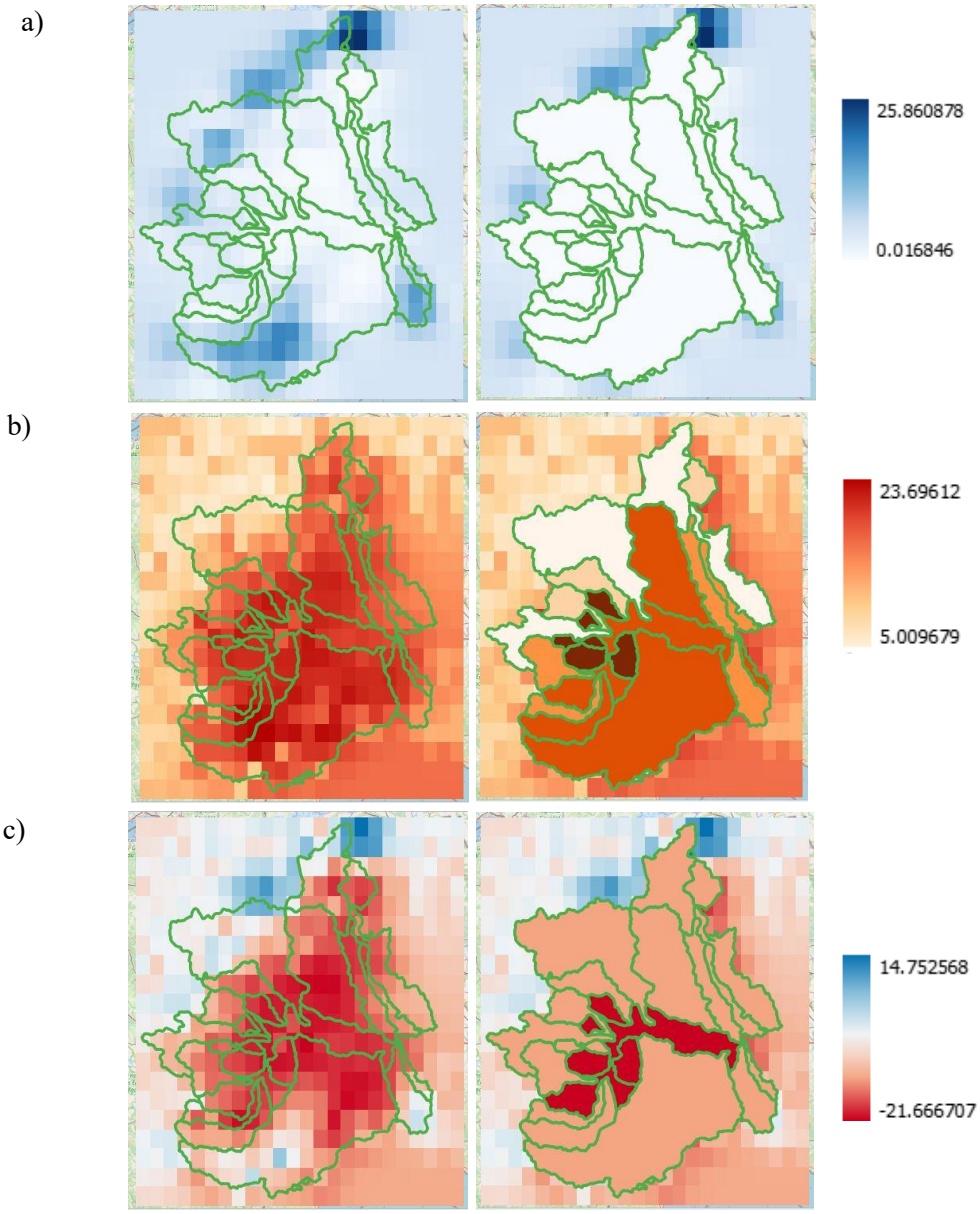

Figure 4-4 a) P (mm) b) PET (mm) c) D (mm) in January 2000

Obtained the spatial average values of monthly P, PET, and D for each basin, we plot them in time, investigating possible trends and non-stationarities.

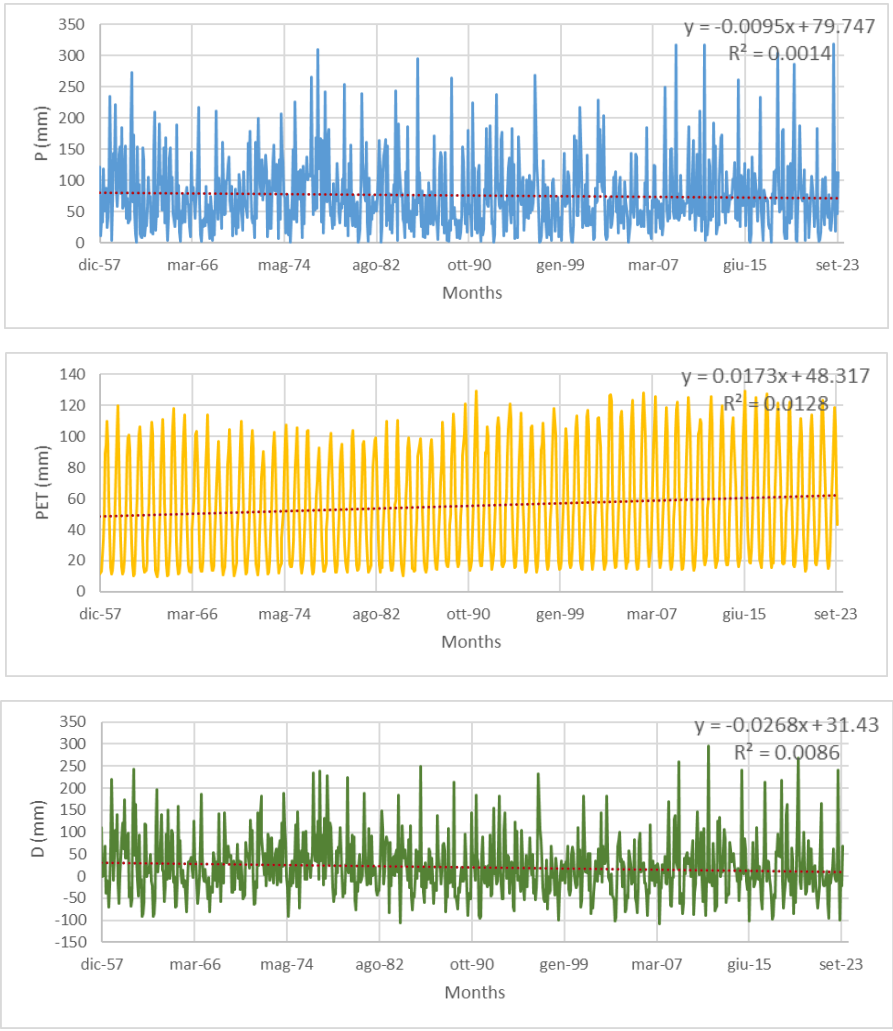

Figure 4-5 Average P, PET and D monthly timeseries Varaita River

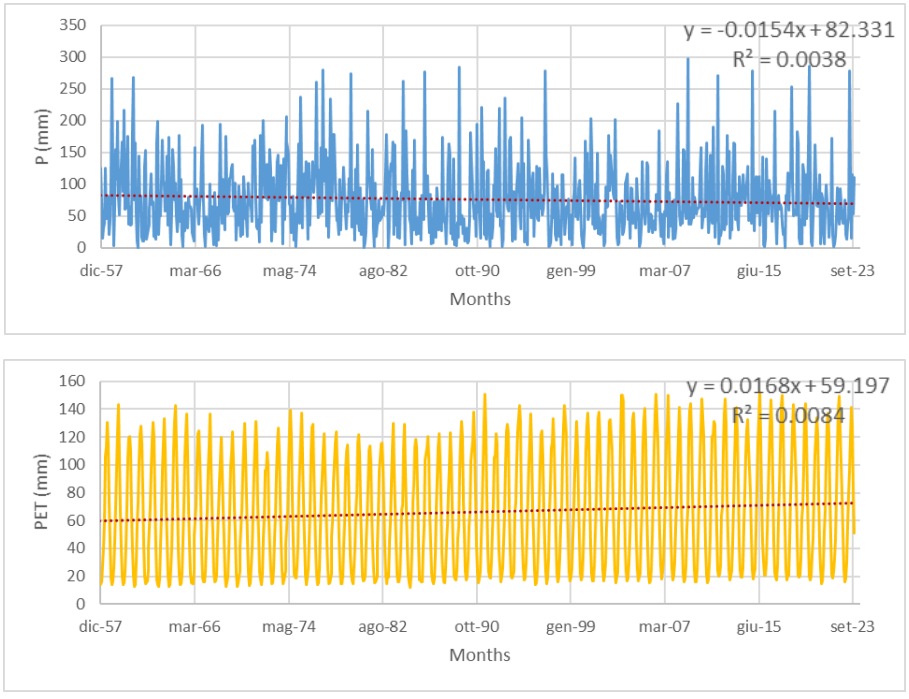

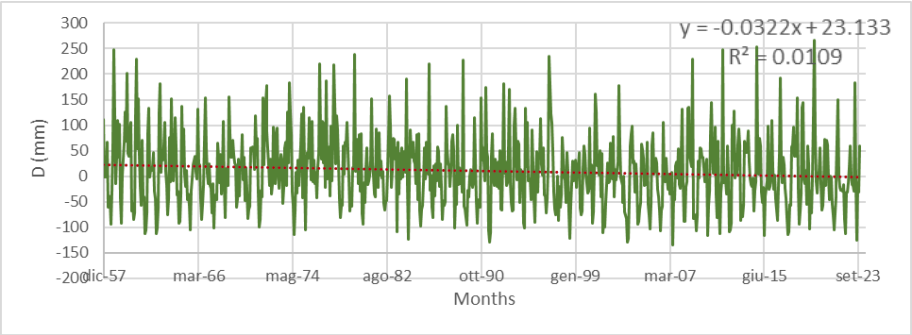

Figure 4-6 Average P, PET and D monthly timeseries Maira River

Figure 4-7 Average P, PET and D monthly timeseries Tanaro River

	P slope (mm/month)	P difference (1957-2022) (mm)	PET slope (mm/month)	PET difference (1957-2022) (mm)	D slope (mm/month)	D difference (1957-2022) (mm)
Varaita	-0.0095	**-7.515**	0.0173	**13.684**	-0.0268	**-21.199**
Maira	-0.0154	**-12.181**	0.0168	**13.289**	-0.0322	**-25.470**
Tanaro	-0.0089	**-7.040**	0.0079	**6.249**	-0.0168	**-13.289**

Table 4-1 Linear interpolation results and P, PET and D difference between 1957 and 2022

Applying a linear regression to the three timeseries for each catchment we can clearly observe the temporal trends of the three hydroclimatic variables, that almost present the same behaviour for all the catchments. Precipitation has kept decreasing in the three basins and Potential Evapotranspiration has increased until today. These two contemporary phenomena have led to a critical decrease in the Water Balance D in all the catchments as we can see in the Table 4-1. These results agree with most of the researchers cited in Chapter 1.3. As far as precipitation is concerned, Pavan et al., 2019, who analysed daily precipitation data from stations in north-central Italy over the period 1961-2015, detected a decrease in precipitation, particularly in the summer period in the northwestern Po Valley, with a decrease in rainy days and an increase in dry periods. While, for example, increasing PET trends find confirmation in studies, such as Falzoi et al., 2019 research. They carried out an analysis on the period 1981-2017 based on precipitation and temperature data from meteorological stations in Piedmont, finding that increasing frequency and duration of drought events is related mainly to increasing temperature and hence, to higher evapotranspiration demand. According to our analysis, the resulting Water Balance (D) shows a significant decrease due to both the climatic factors.

The use of the netCDF files allows to make a first visual analysis of SPEIs values spatial distribution in the study area, for example of the driest years that we briefly analysed in Chapter 1.3.1. Here we present the comparison between SPEI-12 values during 2003, 2010 and 2022 years.

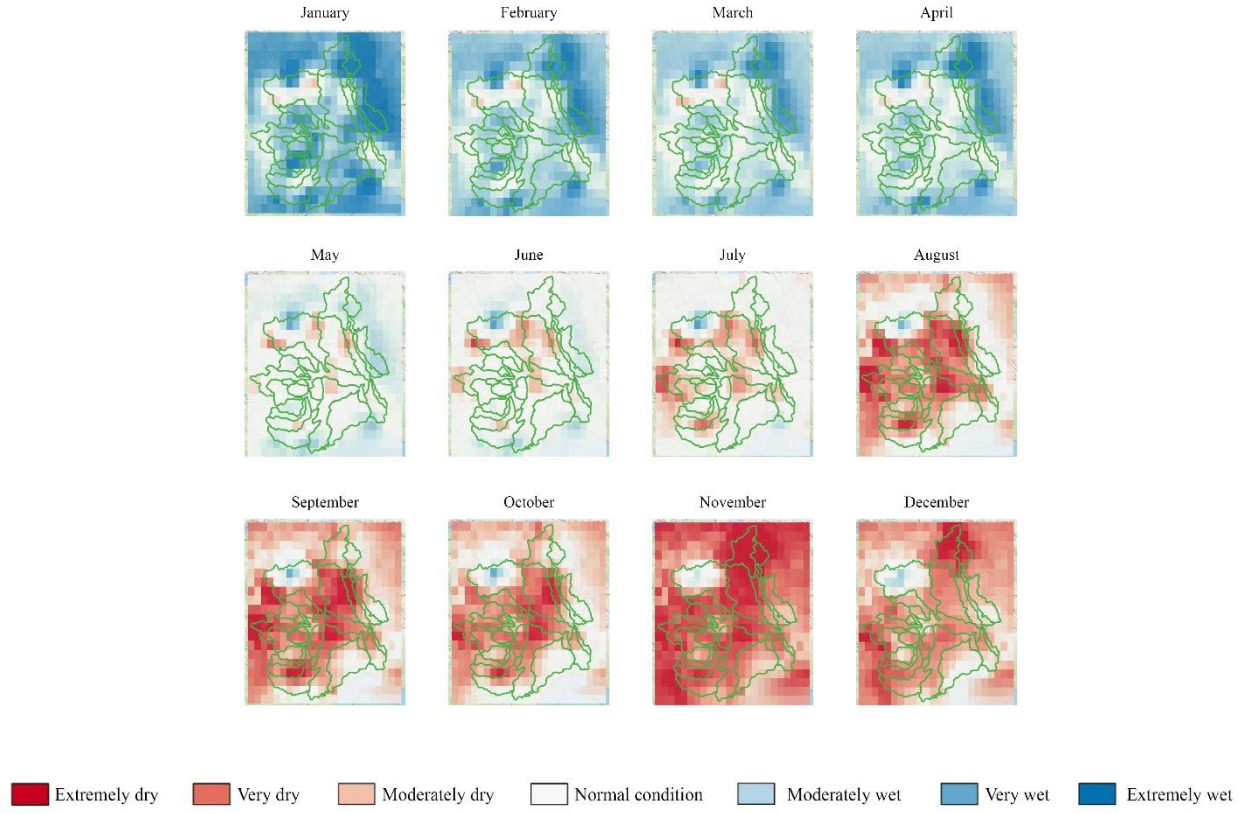

Figure 4-8 SPEI-12 monthly distribution 2003

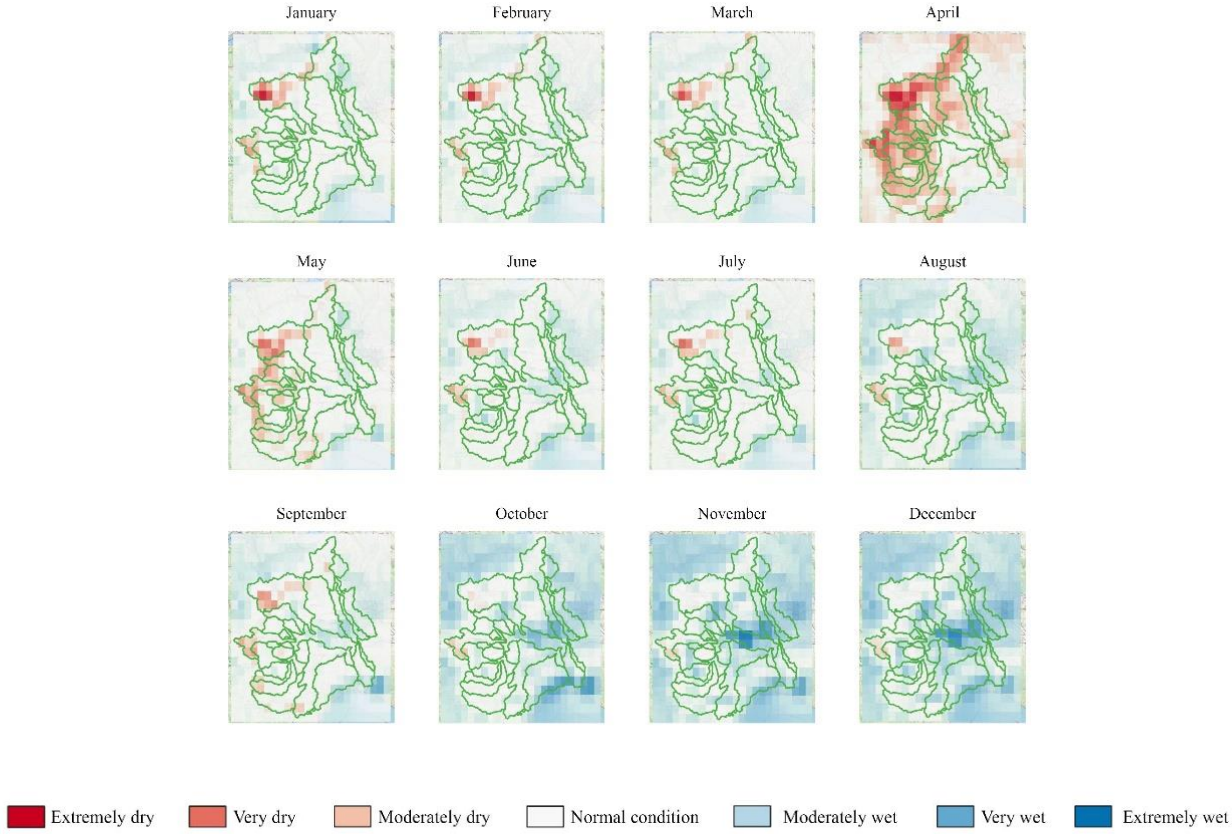

Figure 4-9 SPEI-12 monthly distribution 2010

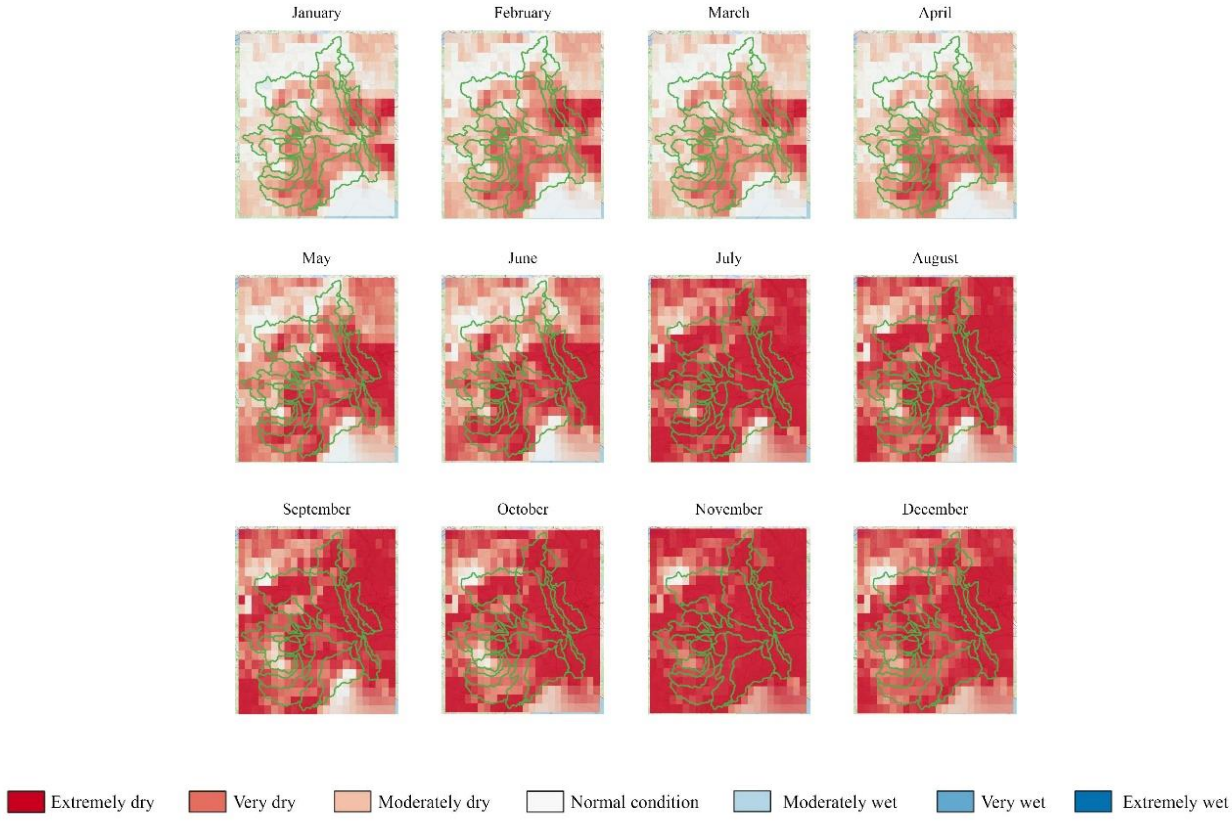

Figure 4-10 SPEI-12 monthly distribution 2022

As shown in the tables above, the results reflect the studies conducted by researchers described in Chapter 1, and specifically, the study conducted by Baronetti at al. in 2020. Here we compare SPEI-12 distribution of two years affected by extreme/severe drought 2003 and 2022 with SPE-12 distribution of 2010. The latter was a "cold" year with an average negative temperature anomaly of about 1°C relative to climate references. Observed rainfall was well above the reference climate, with excess annual accumulation averaging around 40%, also recorded over all provincial capitals. In particular, the annual cumulative exceeded its normal threshold in early May and remained above the reference climate throughout the rest of the year. [S16] In fact, we can observe that since May to the end of the year the SPEI-12 increases in the whole area of Piedmont, achieving moderately and extremely wet condition values mainly in the central and eastern regions of Piedmont. On the contrary, looking at 2003 and 2022 the SPEI-12 rapidly decreases during the year. While in 2003 the average starting conditions in January are very/moderately wet, in January 2022 almost the whole region is already in dry conditions. From July approximately the whole region suffered of extremely dry conditions, which led to critical consequences in water management and in many socio-economic sectors.

QGIS “zonal statistics” function has been exploited also to compute the spatial average of SPEIs within the basins. After having reported the spatial distribution as grid data, here we show the comparison of the average means at basin scale of SPEI-12 of January, March, July and October in the years 2010 and 2022. (Figure 4-11)

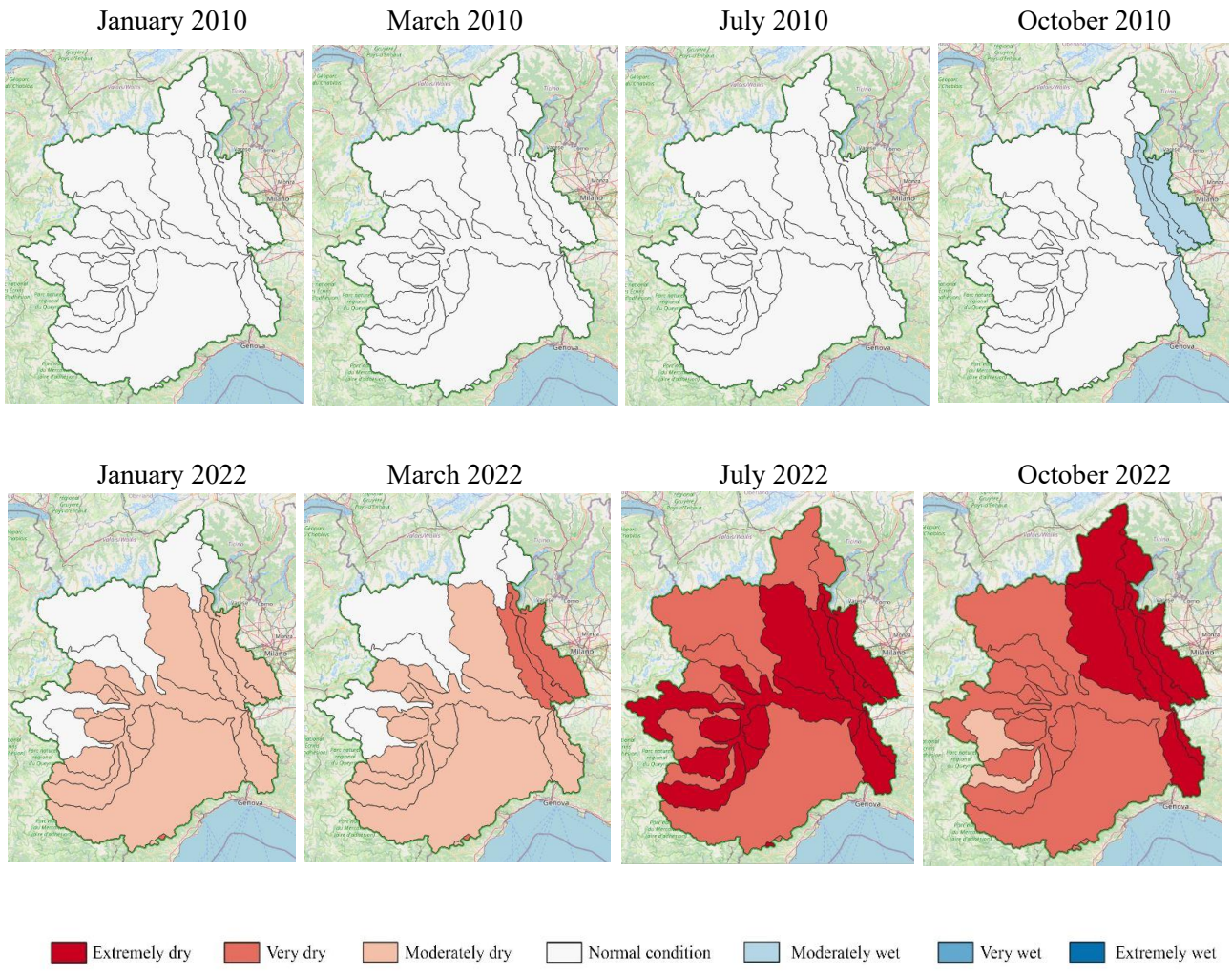

Figure 4-11 Comparison of the average SPEI-12 of January, March, July, and October between 2010 and 2022

We clearly see the different drought conditions among the two years. In 2010 the mean SPEI-12 values are in normal condition or in moderately wet condition. Instead, in 2022 drought criticality increases in time,

affecting only some of the basins in January and growing in all the basins until December, marking very and extremely dry values in most of the basins.

4.2 Streamflow data

4.2.1 Data source

Streamflow series is the base dataset to compute the monthly SSI for each catchment. The first step in the research of streamflow data is related to the choice of the hydrometric stations within the catchments. In order to consider the whole drainage area of the catchment the gauges selected are the nearest to the closing section of each basin. We download the daily streamflow data available in Arpa Piemonte site:

- *Varaita River with closing section at Palonghera:* Daily streamflow data in m3/s, 1st January 2003 – 31st December 2022. Altitude: 246 m a.s.l.
- *Maira River with closing section at Racconigi:* Daily streamflow data in m3/s, 1st January 2003 – 31st December 2020. Altitude: 259 m a.s.l.
- *Tanaro River with closing section at Montecastello:* Daily streamflow data in m3/s, 1st January 1996 – 31st December 2022. Altitude: 84 m a.s.l.

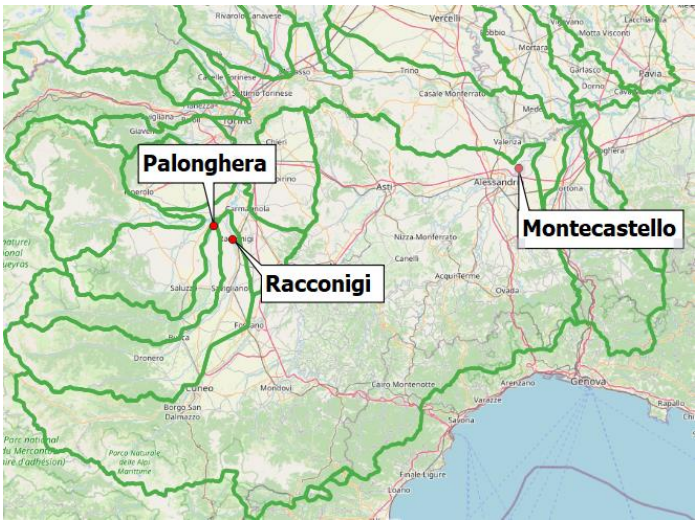

Figure 4-12 Closing sections of the Varaita, Maira and Tanaro basins

4.2.2 Data analysis

The acquired daily streamflow data have been plotted to visualize the order of magnitude of the streamflow of each river and to have a first visual inspection of possible temporal trends (Figure 4-13).

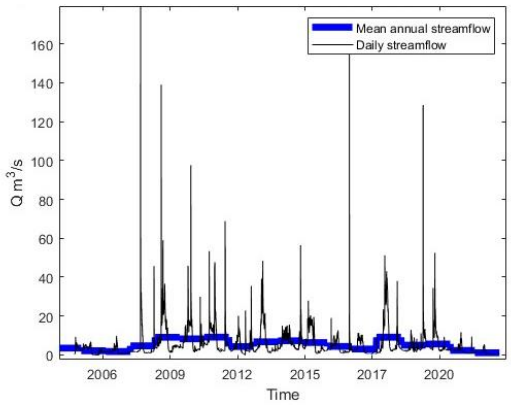

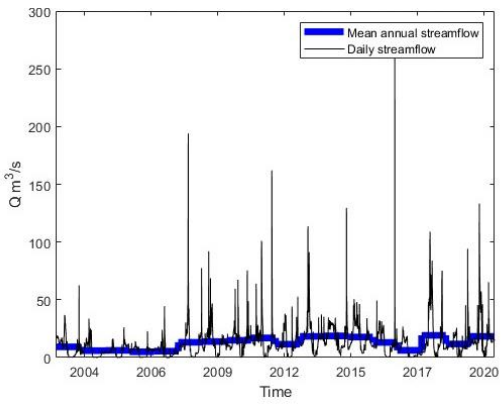

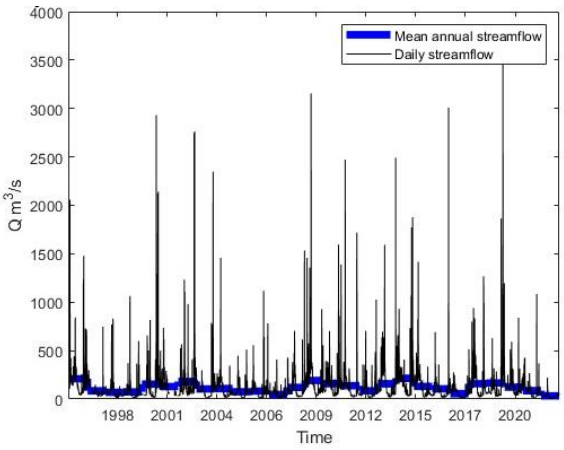

Figure 4-13 Mean annual streamflow and daily streamflow of the Varaita (top left), Maira(top right) and Tanaro (bottom) rivers at the closing sections

	Mean (m3/s)	St. dev (m3/s)
Varaita	5.264	7.756
Maira	12.532	13.498
Tanaro	119.918	182.941

Table 4-2 Mean and Standard deviation of daily streamflow of Varaita, Maira and Tanaro rivers

From the Figure 4-13 and the statistics reported in Table 4-2, we can observe that the Maira and Varaita rivers are much smaller water courses than the Tanaro River (mean values of one/two order of magnitude lower), with very low average discharge, characteristic of torrential/temporary rivers.

We proceed averaging the daily flows on monthly scale in order to obtain the mean monthly discharge (m3/s) timeseries for each river. This allows to work and analyse the hydroclimatic variable needed to then compute the SSI, according to Vicente-Serrano., 2012 methodology. We plot the timeseries of monthly flows for the three rivers (Figure 4-14).

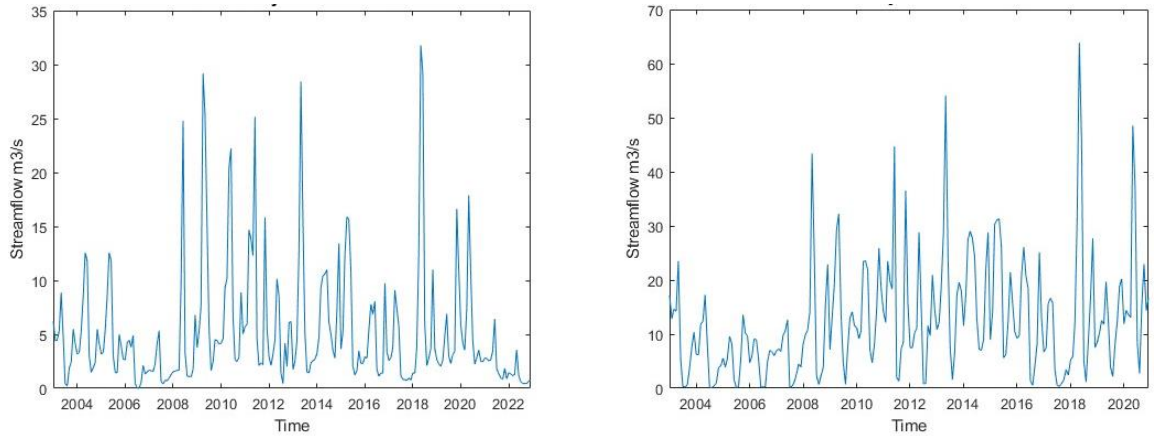

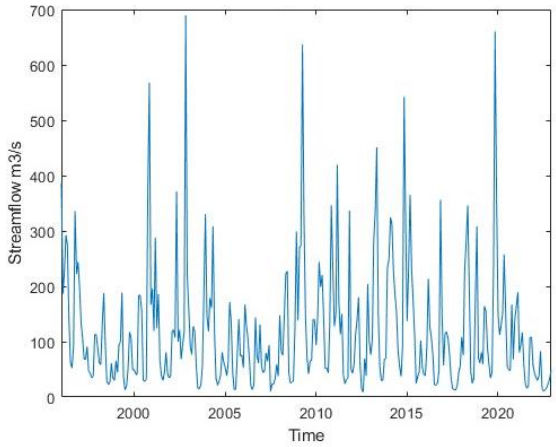

Figure 4-14 Mean monthly streamflow of the Varaita (top left), Maira (top right) and Tanaro (bottom) rivers

We plot the regime curves for each year to indagate the seasonal flow variations among the year. From the regime curves we can observe the same behaviour for the three rivers. Seasonal discharge peaks occur in spring and autumn (May and November) due to peaks in precipitation and snow melt and the low flows during summer (July-August) due to high temperature and low precipitation, as expected from the climatic characterization of Chapter 2.

	Varaita		Maira		Tanaro	
	Mean (m3/s)	St. dev (m3/s)	Mean (m3/s)	St. dev (m3/s)	Mean (m3/s)	St. dev (m3/s)
January	3.167	1.433	8.985	3.292	115.321	79.043
February	3.345	1.434	9.978	3.651	120.159	72.719
March	5.276	3.628	15.152	6.882	161.895	108.357
April	8.501	6.516	18.923	8.388	174.224	115.674
May	12.564	8.371	27.398	16.029	191.462	101.712
June	11.780	8.047	18.848	13.634	102.463	54.543
July	3.060	2.126	3.494	3.648	38.916	26.472
August	1.488	1.122	1.744	2.137	29.937	15.343
September	1.903	1.041	6.270	4.257	45.211	29.173
October	2.399	1.291	10.390	6.607	103.269	88.403
November	5.483	4.780	16.275	9.257	208.786	200.158
December	4.143	3.306	13.021	7.108	140.645	103.130

Table 4-3 Mean and Standard deviation for each month timeseries of the three rivers

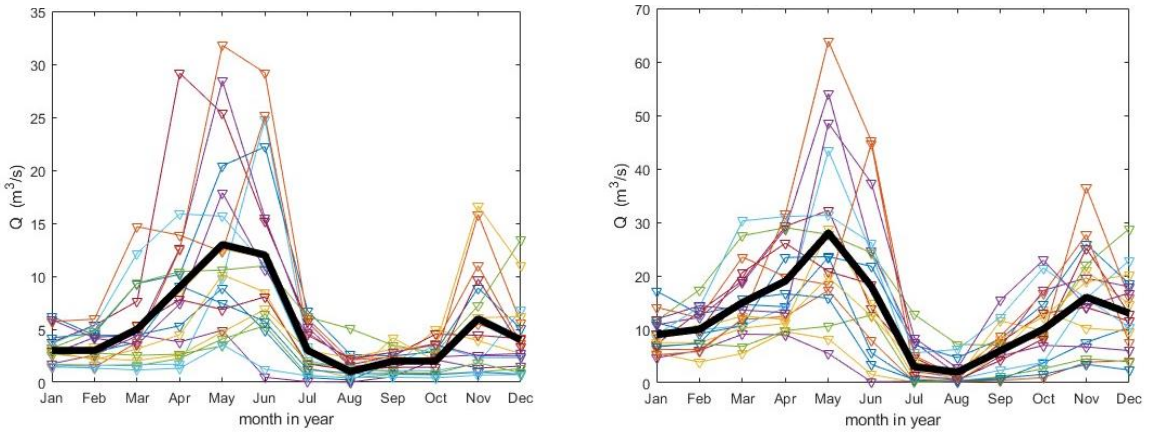

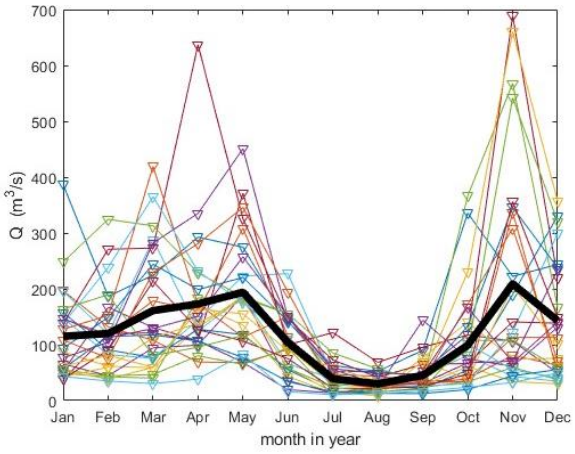

Figure 4-15 Regime curves and mean regime curves of the Varaita (top left), Maira (top right) and Tanaro (bottom) rivers

In this first analysis of the data, we also report the flow duration curves in semi-log scale for the three rivers. Flow duration curve (FDC) is a cumulative frequency curve that shows the percent of time specified discharges are equalled or exceeded during a given period. It combines in one curve the flow characteristics of a stream throughout the range of discharge, without regard to the sequence of occurrence. (Searcy, J.K., 1959)

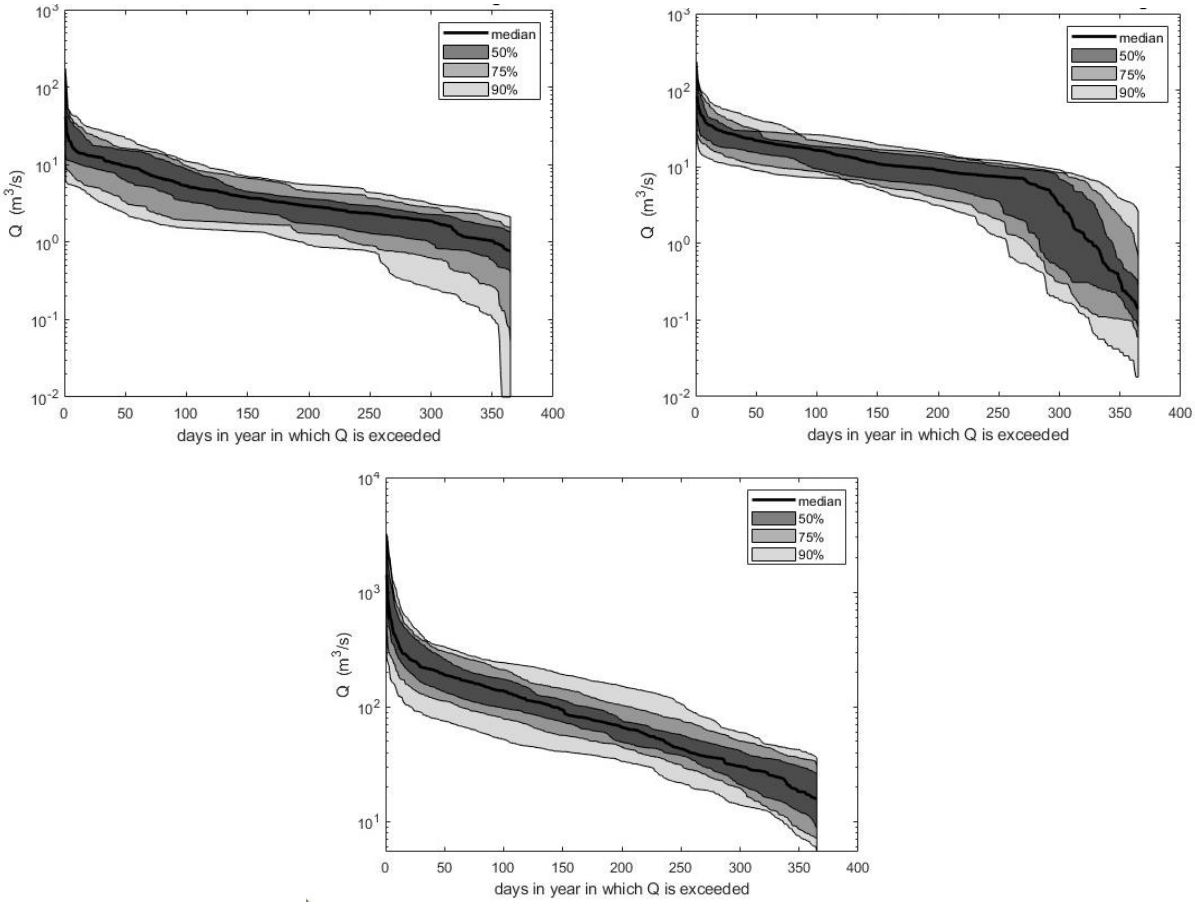

Figure 4-16 Flow duration curves of the Varaita (top left), Maira (top right) and Tanaro (bottom) rivers

The FDCs here reported show the median value and the variability of the values that fall respectively within 50%, 75% and 90% of the total values. In this way, FDCs are useful to indagate the inter-annual end intra-annual variability. In fact, the Varaita River presents a low steepness, meaning that the intra-annual variability is not high. For the Maira River FDC we can observe a high inter-annual and intra-annual variability for low flows. Instead, the Tanaro River shows in general a steeper slope (high range of values) and a quasi-constant inter-annual variability for all the durations.

5. Results

In the previous chapter, we provided a brief analysis of the data used to obtain the results that will be presented in this chapter. Regarding precipitation and temperature data, the monthly values of precipitation (P), monthly potential evapotranspiration (PET), and monthly soil water balance (D) were derived. Subsequently, their spatial distribution and temporal trends were investigated over the period from 1957 to 2023. However, the available discharge data cover a shorter timeframe, approximately the last two decades, for all three considered hydrometric stations. The discharge data were analysed throughout the entire observation period to identify potential trends. In a subsequent phase, the seasonality and flow regimes of the three rivers were studied. It is essential to highlight that the observation period for discharge is significantly shorter than the minimum number of years recommended for robust statistical results. Only for the Tanaro River does the timeframe nearly reach the minimum accepted by the World Meteorological Organization (30 years); indeed, the Tanaro River's Montecastello discharge time series spans 27 years. The observation periods for the Varaita River at Palonghera and the Maira River at Racconigi are 20 and 18 years, respectively. This results in a weaker level of confidence, particularly for the calculated indices for these two rivers. Despite this, the indices can be computed, bearing in mind the lower reliability of the results and the statistical limitations due to the restricted sample sizes.

Now, we proceed moving on to the presentation of the results obtained for the Standardized Precipitation-Evapotranspiration Indices (SPEIs) and the Standardized Streamflow Index (SSI) across the three basins. Subsequently, we will delve into the results of the correlation between these two indices over the entire period and on a monthly scale.

5.1 SPEIs ans SSI results

As described in Section 3.1, the Standardized Precipitation-Evapotranspiration Index (SPEI) is computed for various temporal scales. The variable D (monthly soil water balance) is standardized by calculating the mean and standard deviation over a moving window that considers values of the variable in the preceding months, including the current month for which the index value is calculated. In our case, SPEIs were computed for aggregation periods of 1, 3, 6, 9, 12, and 24 months. The SPEI at different temporal scales holds different meanings, and to interpret the results, it is useful to analyse their individual characteristics. In interpreting the SPEI, it is important to consider that a longer aggregation period provides a better understanding of the drought phenomenon in its entirety and throughout its duration. Short aggregation periods (SPEI-1, SPEI-3) can be misleading and often indicate very high or very low SPEI values even during a period that actually exhibits an opposite trend. To clarify the correct understanding of the results obtained, we rely on the interpretation of the Standardized Precipitation Index (SPI) as described by the World Meteorological Organization (WMO) [S17], with necessary distinctions, as in this case, the standardized variable is the difference between Precipitation and Potential Evapotranspiration:

- SPEI-1

  The SPEI-1 reflects short-term soil water balance values, capturing the soil moisture conditions and water stress for vegetation. As it is linked to the value obtained for the individual month, it can exhibit high or low values even for small variations.

- SPEI-3

  The SPEI-3 provides a seasonal estimate of soil moisture conditions, considering a three-month average. It is particularly useful in the agricultural sector for assessing soil moisture states during the growing seasons of crops. However, it should be compared with SPEIs for longer aggregation periods for a comprehensive analysis.

- SPEI-6

The SPEI-6 represents the seasonal and medium-term moisture condition. In other words, it is valuable for recognizing the degree of moisture or drought during a specific rainy season, for example, from October to March. Additionally, it can be useful in identifying the initial signs of water deficit for streamflow and rivers, providing insights into the overall hydrological basin.

- SPEI-9

The SPEI-9 describes inter-seasonal moisture/drought conditions. Given that drought typically takes about a season to manifest, low values of SPEI-9 can indicate that drought is already impacting the agricultural sector and other areas. SPEI-9 begins to detect long-term drought phenomena that may have already translated into hydrological drought.

- SPEI-12 – SPEI-24

From SPEI-12 onwards, long-term drought events (extending to multi-year durations) are detected. Prolonged meteorological drought events (lasting for seasons to years) result in reduced levels not only in surface flows but also in groundwater reserves.

5.1.1 Drought propagation in the study basins

Having established these premises, let us begin analysing the results obtained for SPEI-1 and SSI. Both fundamentally represent the monthly trends of the basin-scale water balance and river discharge, respectively, but in a standardized form. This initial analysis helps define the effects of SPEI values representing moderate, severe, or extreme drought at the monthly scale on the terrestrial hydrological system. Furthermore, our focus in this analysis is on the characteristics of "drought propagation" as described in Section 1.2.

To study the characteristics of drought propagation, namely “Pooling”, “Attenuation”, “Lag”, and “Lengthening”, we considered four meteorological drought events highlighted in the studies mentioned in Section 1.3.1. The events referred to in Figure 5.1 are January 2003 – March 2004, January 2007 – December 2007, January 2017 – December 2017, and January 2022 – December 2022. For the Maira River, discharge data for 2022 are not available, so the last-mentioned period is not included in the study. Let us proceed to analyse the four characteristics and verify their presence in the obtained time series of indices.

The effect of "Pooling," which involves the combination of consecutive meteorological drought events resulting in a prolonged hydrological drought, is clearly visible in the graphs in Figure 5.1. An example can be observed in the graphs related to the Maira River. The meteorological drought events starting from January 2003 until February 2008, interspersed with brief periods of moderate humidity, translated into an extended drought period for the Maira River until April 2008, with peaks even beyond -2. Another example is the SPEI-1, which assumes negative values from November 2006 to February 2008 with brief positive monthly intervals in the Tanaro basin. In this case as well, the streamflows of the Tanaro at Montecastello exhibit conditions of moderate and severe drought throughout the mentioned period. Regarding the "Lag" effect, which represents the delay in hydrological response to meteorological drought (the time between meteorological and hydrological drought), this can be observed in the 2003 drought event. For the Varaita and Maira rivers, the drought was detected with a two-month delay, while for the Tanaro, it was one month delayed. However, in the 2017 drought period, a longer duration of drought compared to the meteorological one ("Lengthening") is observed for all rivers. The same applies to the Varaita and Tanaro in the 2022 event. Another phenomenon that can be observed is "Attenuation." For example, while SPEI-1 often shows values below the -2 threshold (beyond which drought is defined as extreme), SSI values tend to have peaks indicating "severe" drought and rarely "extreme" drought. However, as noted earlier, the SSI oscillations are lower (pooling), as the basin system acts as a filter, dampening sudden variations that are frequent in meteorological phenomena. For this reason, SPEIs were calculated for longer time scales to understand which climatic drought time scale can effectively describe the response time of the hydrological basin.

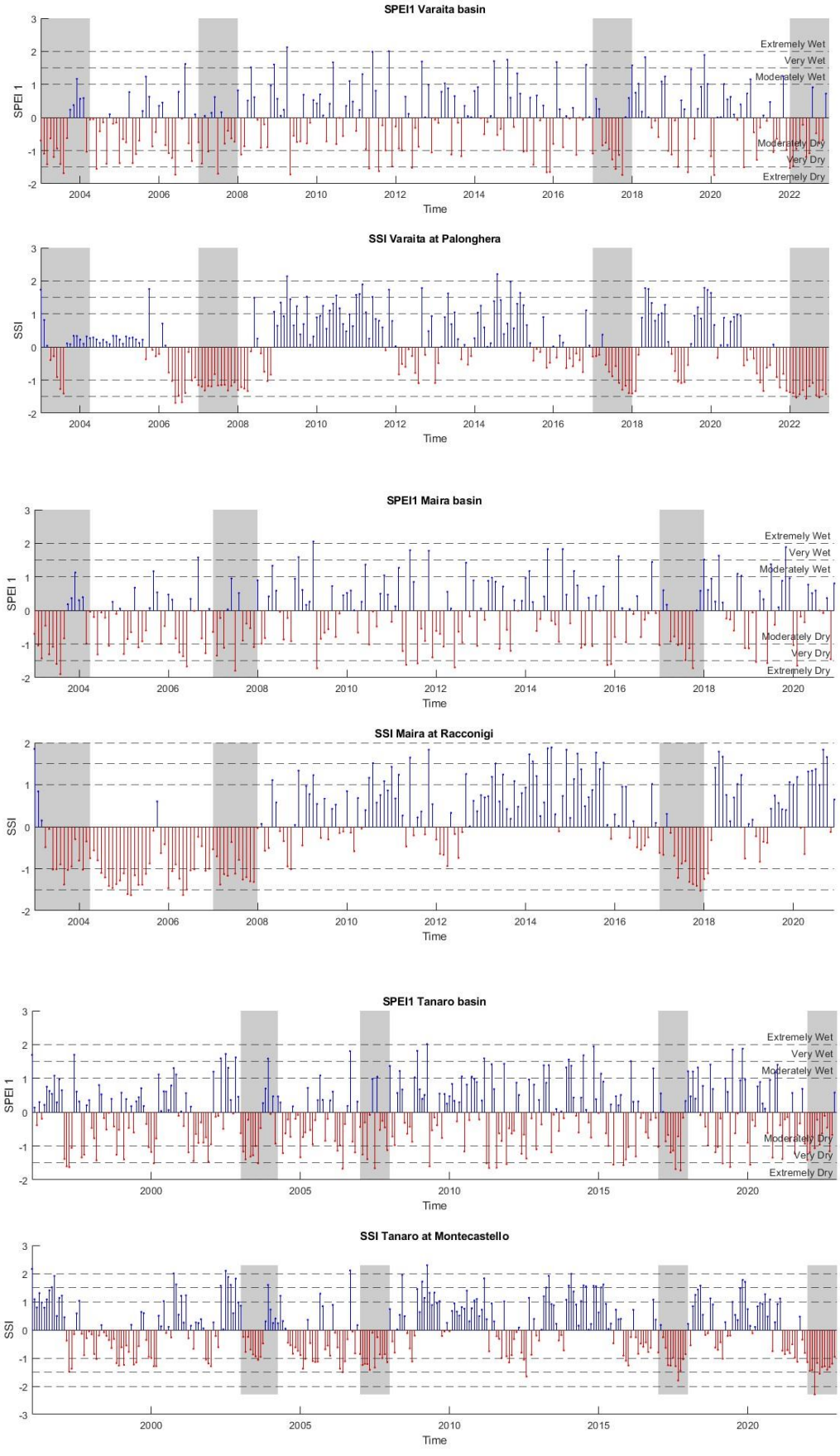

Figure 5-1 SPEI 1 and SSI timeseries for the three basins

5.1.2 SSI and SPEIs timeseries and “drought runs”

With these premises, Figure 5.2 presents the graphs of the SSI and SPEIs for an initial visual analysis of the obtained results. We can observe that the SSI shows a temporal evolution with medium-term fluctuations on average, while the SPEIs exhibit different oscillations depending on their temporal scale. The larger the temporal scale, the lower the frequency of oscillations.

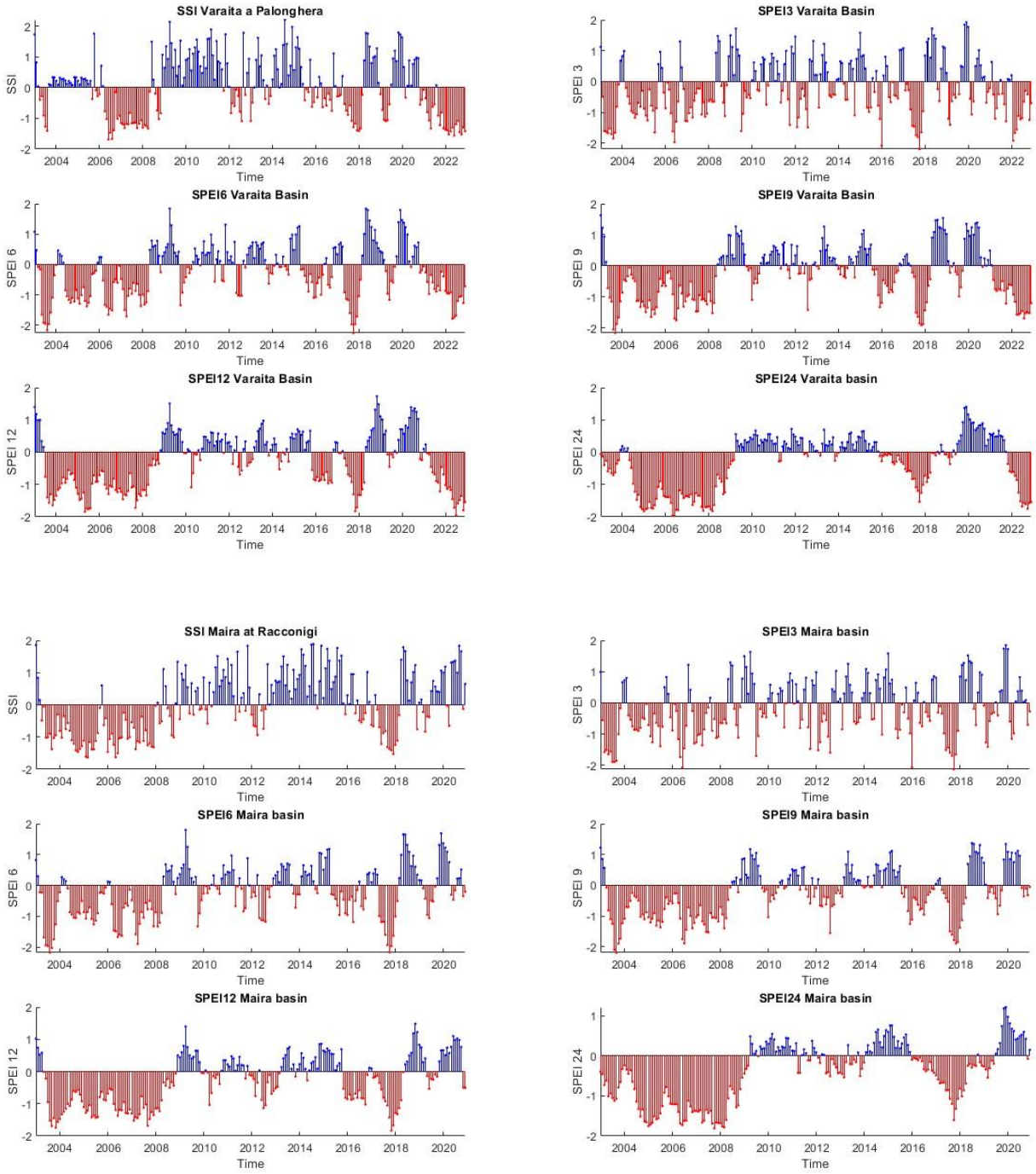

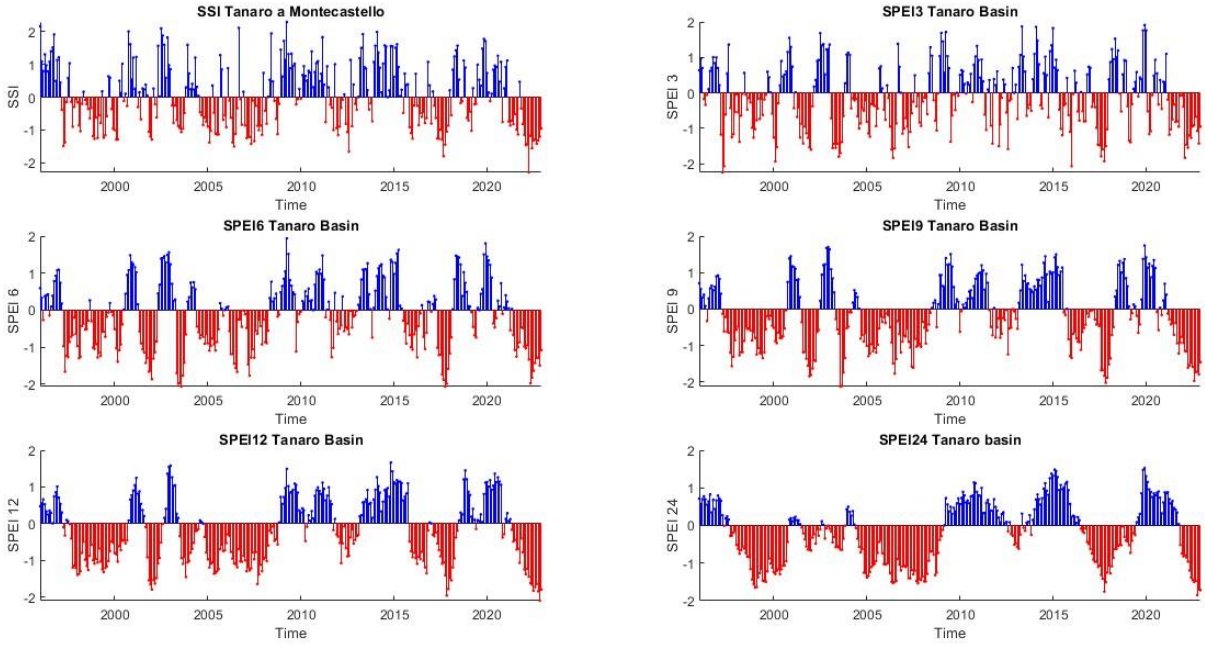

Figure 5-2 SSI and SPEIs timeseries of the three basins

Moreover, since the Maira River basin and the Varaita River basin are adjacent and, therefore, have experienced similar meteorological conditions over time and share morphological similarities in terms of lithological structure and physical characteristics (average elevation, area, length of the main river channel, etc.), we can observe a similar trend in both SSI values and SPEI values for different aggregation periods.

To study drought periods more accurately, we implement the "drought runs" analysis, mentioned in Section 3.1. Through this analysis, drought events, their duration, water deficit, and the intensity of each event are identified. Below are the meanings of each of these attributes:

- Drought Duration: The length of the drought event.
- Drought Severity (Deficit): The sum of index values during the drought event.
- Drought Intensity: The ratio of severity to the duration of a drought event.

In our study, it is important to note that a single drought event is defined by the SPEI value falling below -1, which is considered the threshold, and the event concludes when the value rises above 0 (specifically at least one standard deviation below the mean and the mean itself).

By implementing the "drought runs" analysis, we observe that for all basins, drought periods become progressively longer and more severe as the temporal scale of the SPEI increases, indicating increasingly substantial water deficits. This trend was already evident in the simple graphs containing the time series but is confirmed by the results of the "drought runs" analysis. Below are the values reported for SPEI-1, SPEI-6, and SPEI-12 for the Maira River and Tanaro River basins as examples (the time series of SPEIs for the Maira and Varaita River basins show a similar pattern).

	Event 1	Event 2	Event 3	Event 4	…	Event 24	Event 25	Event 26	Event 27
Duration (months)	8	4	3	3	…	4	1	4	1
Deficit	-9.616	-2.633	-2.787	-2.611	…	-3.839	-1.565	-3.199	-1.451
Intensity (1/months)	-1.202	-0.658	-0.929	-0.870	…	-0.960	-1.565	-0.800	-1.451

	Event 1	Event 2	Event 3	Event 4	Event 5	Event 6	Event 7	Event 8
Duration (months)	9	17	25	7	7	3	9	4
Deficit	-13.499	-12.996	-26.015	-3.322	-4.984	-1.818	-13.136	-2.089
Intensity (1/months)	-1.500	-0.764	-1.041	-0.475	-0.712	-0.606	-1.460	-0.522

	Event 1	Event 2	Event 3	Event 4	Event 5
Duration (months)	64	6	9	2	9
Deficit	-67.865	-2.525	-4.952	-1.126	-10.627
Intensity (1/months)	-1.060	-0.421	-0.550	-0.563	-1.181

Table 5-1 "Run theory" results of SPEI 1, SPEI 6 and SPEI 12 of the Maira basin

	Event 1	Event 2	Event 3	Event 4	…	Event 33	Event 34	Event 35	Event 36
Duration (months)	4	2	1	2	…	1	4	3	11
Deficit	-5.657	-2.590	-1.427	-1.776	…	-1.341	-2.595	-2.237	-8.585
Intensity (1/months)	-1.414	-1.295	-1.427	-0.888	…	-1.341	-0.649	-0.746	-0.780

	Event 1	Event 2	Event 3	Event 4	…	Event 10	Event 11	Event 12	Event 13
Duration (months)	16	11	5	10	…	6	2	10	18
Deficit	-12.870	-8.759	-4.821	-13.383	…	-4.045	-1.664	-14.596	-21.464
Intensity (1/months)	-0.804	-0.796	-0.964	-1.338	…	-0.674	-0.832	-1.460	-1.192

	Event 1	Event 2	Event 3	Event 4	Event 5	Event 6	Event 7	Event 8
Duration (months)	36	10	11	45	12	8	11	15
Deficit	-32.934	-12.108	-8.005	-40.303	-6.228	-7.407	-12.945	-21.644
Intensity (1/months)	-0.915	-1.211	-0.728	-0.896	-0.519	-0.926	-1.177	-1.443

Table 5-2 "Run theory" results of SPEI 1, SPEI 6 and SPEI 12 of the Tanaro basin

5.2 SPEIs and SSI correlation

Investigating the correlation between meteorological drought indices (SPEIs at 1, 3, 6, 9, 12, and 24 months) and hydrological drought (SSI) is the final step of this study and the goal of this thesis. Understanding the relationship between these two phenomena through the correlation of their respective indices for different aggregation periods can help identify the temporal scale related to climatic drought events that best represents the hydrological response time of the basins to such events.

5.2.1 Correlation coefficient at different timescales

In this section, we present the initial results of linear correlation between the SSI index and SPEIs for different aggregation periods.

Time scales over which the SPEI are the most correlated with the SSI are identified as the candidate drought response time. The candidate drought response time is derived by assessing the SPI-SSI relationship. Given that the SPEI-SSI relationship indicates the generalized linkage between precipitation anomalies and streamflow anomalies, it implies that water surplus in addition to water deficits is jointly considered. However, efforts to recognize the drought response time is motivated by the practical requirement for drought monitoring, thereby highlighting that the specific focus ought to be laid on deficit aspect of usable water resources.

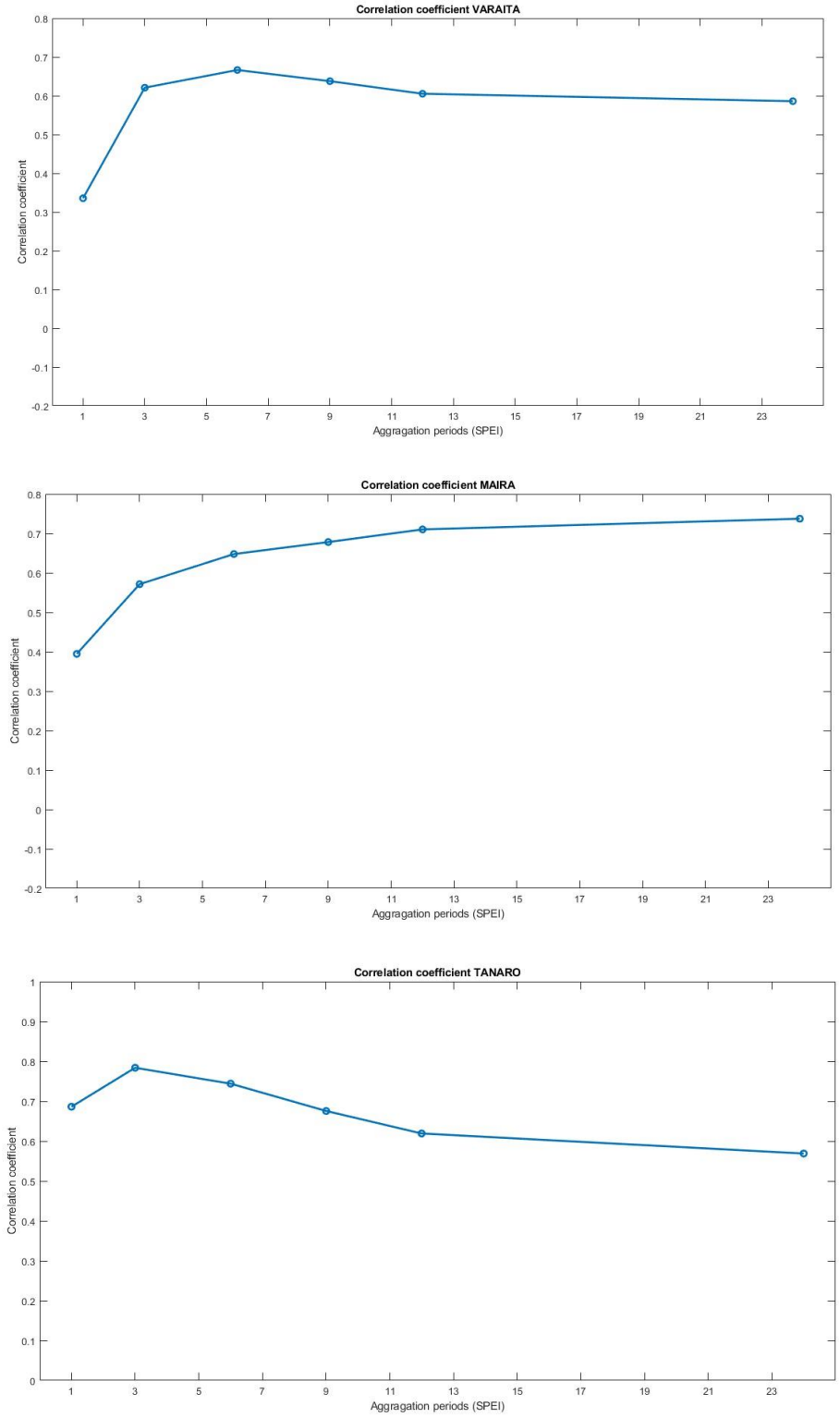

Figure 5-3 Correlation coefficient between SPEIs and SSI

As observed, the correlation between the two indices for different temporal scales is positive and very high for all three basins. However, the basin-specific peak correlation varies: the Varaita River basin exhibits the maximum correlation between SSI and SPEI-6, the Maira River basin between SSI and SPEI-24, while the Tanaro River basin between SSI and SPEI-3. The temporal scale of the SPEI with the highest correlation should be indicative of the basin's response time to climatic moisture/drought inputs. Therefore, we deduce that the Varaita River basin has a response time of around 3-6 months (peaking at 6 months with approximately 0.7) but maintains a long memory up to 24 months (around 0.6). The correlation coefficient for the Maira River basin shows an increasing trend with the aggregation period, reaching a maximum at 24 months (approximately 0.75). This indicates that the basin begins to respond to climatic inputs after three months, but the effects on streamflow are fully evident in the long term. Finally, concerning the Tanaro River basin, there is a peak correlation of about 0.8 at three months (short basin response), decreasing to 0.6 at 24 months (still maintaining good long-term memory). A similar trend is observed for the Varaita and Tanaro River basins. These results are somewhat unexpected and warrant further discussion, which will be explored in the next section, where the correlation coefficient between SPEIs and SSI for each month of the year will be analysed.

5.2.2 Monthly correlation coefficient

The basin's response time can vary seasonally, influenced by a multitude of factors. Primarily, factors such as soil moisture levels and the groundwater level before a precipitation event play a crucial role. Another significant factor is the cycle of snow formation and melting in the Alpine region (Maritime and Cottian Alps) and occasionally in the pre-Alpine areas. This cycle strongly affects the streamflow regime for all three basins, especially in autumn and spring, and needs to be considered when interpreting the correlation between SPEIs and SSI indices.

The Varaita River basin exhibits a highly variable response time depending on the considered temporal scale and month (general range -0.18 to 0.83). The only values of the correlation coefficient that are very low and even negative are those between SSI and SPEI-1 for the months of January and February (winter), April and May (spring), and August and September (summer). Here is a summary of the temporal trends of the correlation coefficient:

- January, February, and March show a relatively constant trend, with low values only for SPEI-1, hovering in the range of 0.5-0.7.
- April, May, June, and July peak between three and six months (0.7-0.8) and then decrease over the long term.
- August and September increase with the temporal scale (up to 0.7).
- October remains constant at values between 0.4-0.6.
- November and December peak at three months (0.8) and then slightly decrease up to 24 months (minima of 0.7).

In conclusion, the Varaita River basin responds in the short-term during spring and autumn, in the long-term during summer, and from the medium-term onwards in winter.

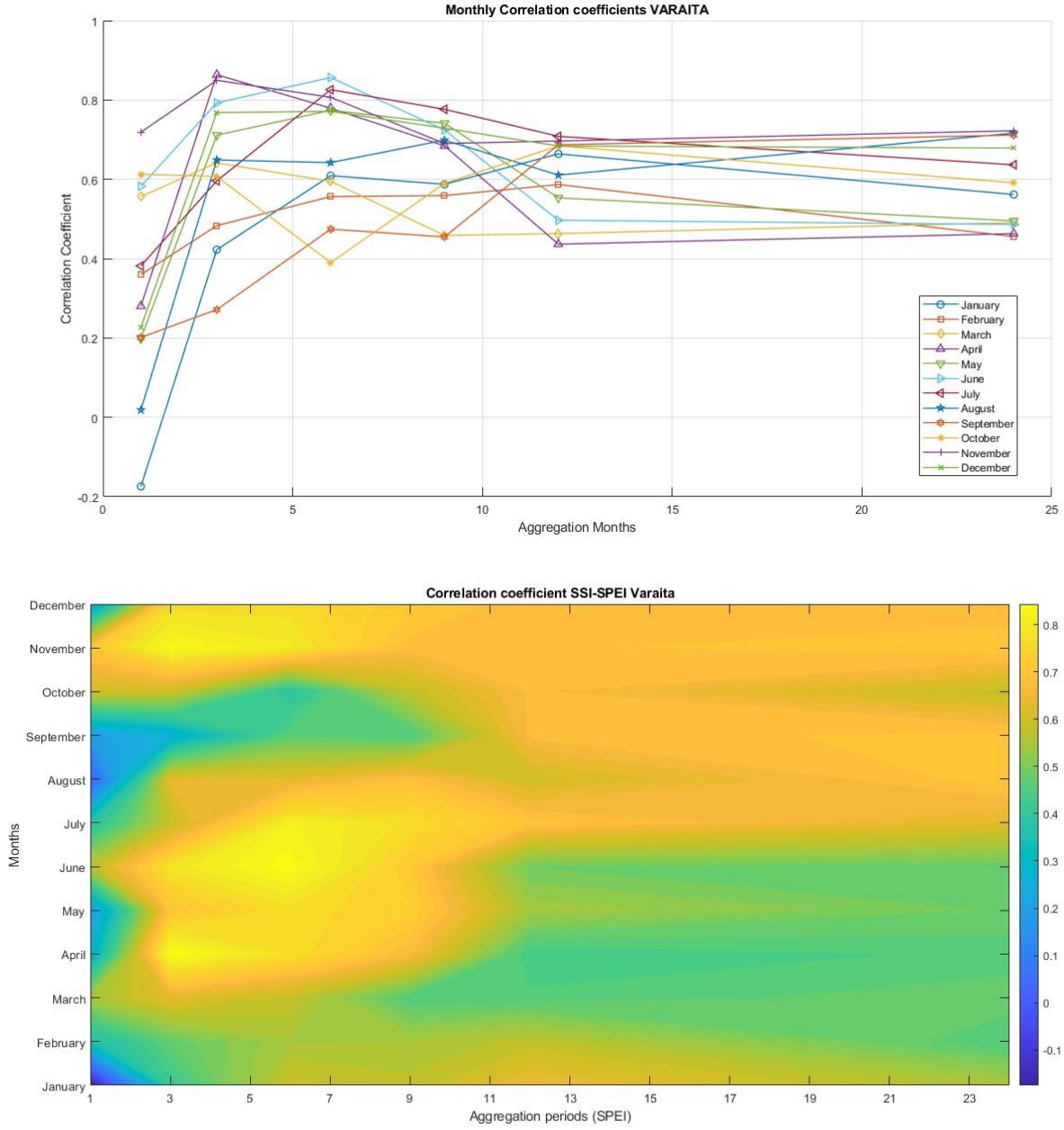

Figure 5-4 Correlation coefficient between SPEIs and SSI for each month, Varaita basin

Similarly, the Maira River basin exhibits a highly variable response time depending on the considered temporal scale and month (general range -0.18 to 0.85). In this case as well, the correlation coefficient assumes the lowest values (-0.18 – 0.2) between SPEI-1 and SSI. Here is a summary of the seasonal trends:

- From January to March, there is an increase in correlation up to the 12-month temporal scale, where a peak is observed (0.8), followed by a decrease in the long-term response (down to 0.6).
- April shows a different trend with a peak at 3 months (0.82) followed by a decrease in the medium and long term.
- From May to December, the trend is generally an increase in the coefficient in the long term. The only difference is that there is an average of values around 0.5 for temporal scales of 6-9 months for the months of August, September, and October.

In general, we can state that the basin's response to climatic inputs has a medium to long-term temporal scale.

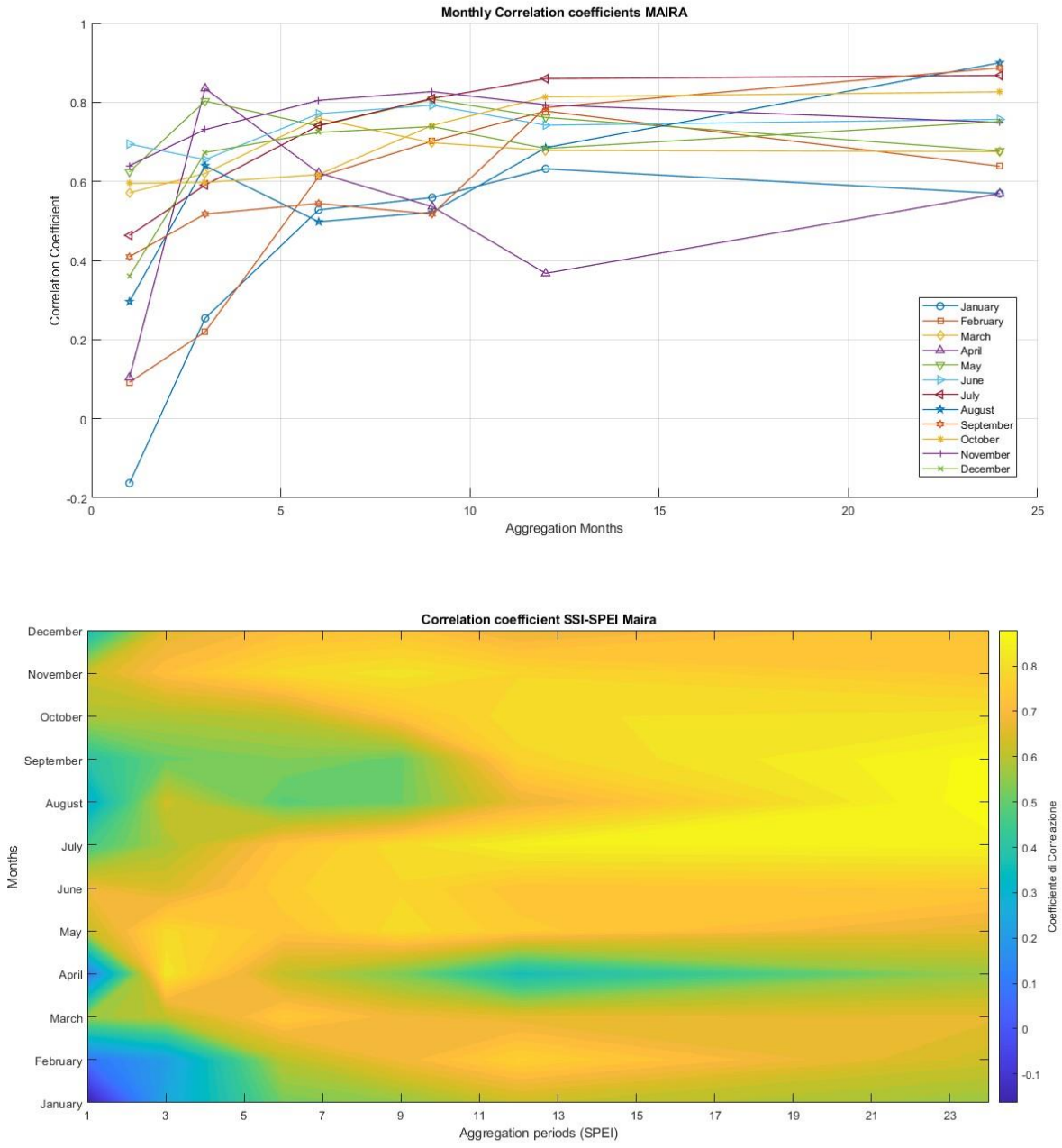

Figure 5-5 Correlation coefficient between SPEIs and SSI for each month, Maira basin

The Tanaro River basin exhibits a generally narrower range of correlation coefficients (0.4 – 0.9). This indicates that the overall response of the basin to climatic inputs is quite high for all temporal scales. In detail:

- January shows constant values in the short and medium term of about 0.7, decreasing in the long term.
- From February to May, there is a peak in short-term correlation at three months (over 0.85) and a decrease in the long term.
- June, July, and August remain constant for all temporal scales.
- From September to December, the correlation is very high in the short and medium term, i.e., from 1 to 6 months of aggregation, and decreases in the long term.

In general, we can conclude that the hydrological response of the Tanaro River basin to climatic inputs is very short (1-3 months) compared to the other two studied basins.

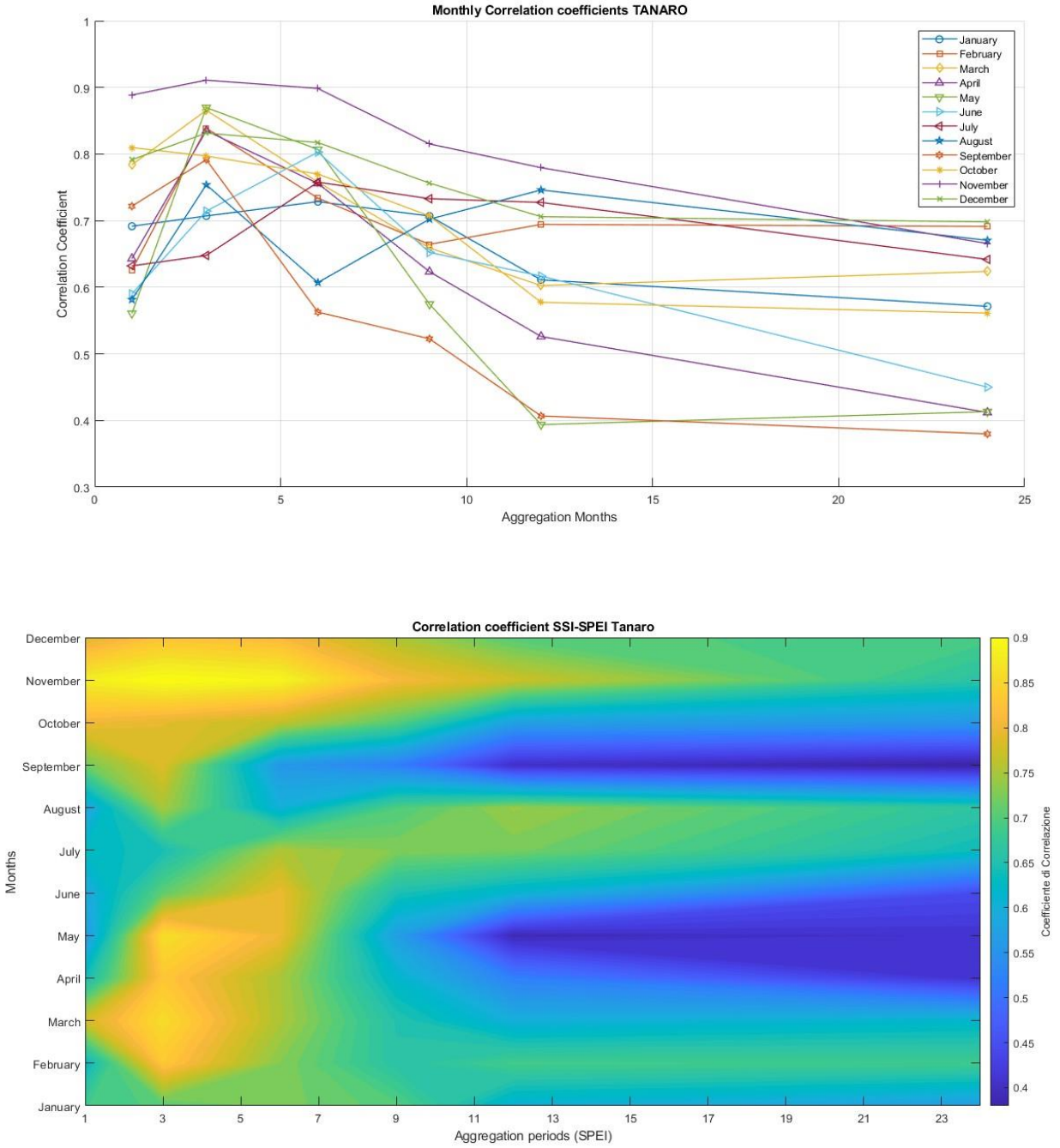

Figure 5-6 Correlation coefficient between SPEIs and SSI for each month, Tanaro basin

6. Conclusions

The goal of this thesis has been to investigate the hydrological response of the southern Piedmont basins to meteorological drought ("drought propagation"). To achieve this, an analysis based on climatic and hydrological drought indices calculated at the basin scale was adopted. The methodology used included, first and foremost, the collection of monthly climatic data (precipitation P and temperature T) within the study basins and the monthly river flows recorded at closing sections. From the time series of precipitation and temperature, potential evapotranspiration (PET) was calculated, followed by the monthly soil water balance D (P – PET). Subsequently, the Standardized Precipitation Evapotranspiration Index (SPEI) values were calculated for various temporal scales, along with the Standardized Streamflow Index (SSI), providing standardized monthly flow values. Finally, the correlation between the two indices was verified by calculating the linear correlation coefficient between them. The underlying assumption for implementing this strategy is that flow values are correlated over time (though not always linearly) with input values of precipitation and evapotranspiration within the catchments. The main question addressed was the time lag between a climatic drought event and a hydrological drought event (temporal lag). For this reason, the SPEI was calculated for different aggregation periods, as increasing the aggregation time considers the drought event more comprehensively and provides insights into its persistence over time. A prolonged drought event, such as consecutive months or years, can result in a reduction of streamflow and, consequently, a deficit of surface water resources within the basins (hydrological drought). The analysis of the correlation between SPEIs and SSI identified the SPEI temporal scales with the highest correlation with SSI, which likely represent the hydrological response time of the basin.

The obtained results reveal that the three basins respond differently to climatic inputs of humidity/drought. Furthermore, the basin response varies seasonally, often displaying contrasting outcomes. To better interpret the results, in-depth studies on groundwater and piezometric variations in the distinct basins, lithology to derive soil and underlying layer permeability, and the actual regulation level of reservoirs along river courses should be conducted. In this study, we limit ourselves to proposing hypotheses, which should be considered purely qualitative and approximate. Concerning the Varaita and Maira river basins, there is noticeable temporal memory, meaning the basin responds to climatic inputs with a temporal lag of three months (short-term) and maintains a positive response even for longer temporal scales. As predominantly mountainous basins, snow accumulates in the winter and is released as runoff in the spring-summer periods. This could contribute to maintaining a consistently high positive correlation for medium to long-term temporal scales. The Tanaro River basin has much wider area compared to the other two basins, comprehending Po plain in the north-eastern part. This would suggest a longer response time compared to basins with steeper slopes and smaller areas. However, as observed earlier, a short hydrological response time of the basin is detected (1-3 months).

To fully comprehend the obtained results, it would be necessary to extend the analysis to additional basins with diverse geomorphological characteristics and different hydrological and climatic regimes. This approach would allow for the definition of basins classes with similar hydrological response characteristics, enabling a precise investigation into the factors determining the different responses. Considering the non-linear relationships often observed in the hydrological response of basins to preceding climatic conditions (Van Loon and Laaha, 2015; Wang et al., 2016), exploring the relationship between climatic and hydrological drought through non-linear correlation coefficients could be considered. Furthermore, the conducted analysis could be enriched by evaluating trends in the index value time series, especially taking into account autocorrelation phenomena within the data. In any case, the present study provides a solid methodological foundation and has yielded correlation results that are generally satisfactory.

Understanding the phenomenon of drought and studying its propagation within the terrestrial hydrological cycle is of paramount importance in today's context. Drought is a climatic hazard that can affect all types of climates on Earth and can have devastating consequences if it persists over time. According to the latest assessment report (AR6, 2021) from the Intergovernmental Panel on Climate Change (IPCC), drought events in Southern Europe have increased in duration and frequency over the past fifty years, with a high likelihood

of further increases in all Representative Concentration Pathways (RCP) scenarios. Therefore, monitoring drought is essential within the context of climate change adaptation strategies. Predicting the extent and timing of water deficits after a climatic drought event is crucial for developing strategic plans in water resource management. This knowledge can assist populations in adopting adaptive measures to cope with water scarcity. The impacts of drought on society and ecosystems are of significant concern at the European level. In fact, following the adoption of the new "EU Strategy on Adaptation to Climate Change" in 2021, the European Commission launched the "European Drought Observatory for Resilience and Adaptation" (EDORA) project. The aim of EDORA is to enhance resilience and adaptation to drought within the European Union.

"As droughts jeopardize European water resources, understanding the complex impacts and the risks they pose is the first step to safeguard access to water for all people and ecosystems, now and in the future."

(EDORA, JRC 2024)

7. Website

[S1] https://www.arpa.piemonte.it/rischinaturali/approfondimenti/clima/Siccita/siccita_meteo.html

[S2] https://www.arpa.piemonte.it/arpa-comunica/file-notizie/2023/rsa-sintesi-2023-stampa-def-sito.pdf

[S3]https://www.arpa.piemonte.it/rischinaturali/tematismi/clima/rapporti-di-analisi/annuale_pdf/meteo_2003.pdf

[S4]https://www.arpa.piemonte.it/rischinaturali/tematismi/clima/rapporti-di-analisi/annuale_pdf/anno_2017.pdf

[S5]https://www.arpa.piemonte.it/rischinaturali/tematismi/clima/rapporti-di-analisi/annuale_pdf/anno_2022.pdf

[S6] https://www.regione.piemonte.it/web/temi/ambiente-territorio/cambiamento-climatico/cambiamento-climatico-piemonte

[S7] https://files.cmcc.it/ar6/wg2/scienziati_italiani_IPCC_ar6_wg2.pdf

[S8] https://www.adbpo.it/territorio-di-competenza/

[S9]https://www.adbpo.it/PAI/1%20-%20Relazione%20generale/1.1%20-%20Relazione%20generale/RelGenCap_3.pdf

[S11]https://www.adbpo.it/PAI/3%20-%20Linee%20generali%20di%20assetto%20idraulico%20e%20idrogeologico/3.3%20-%20Elaborato%20Piemonte/Maira.pdf

[S10]https://www.adbpo.it/PAI/3%20-%20Linee%20generali%20di%20assetto%20idraulico%20e%20idrogeologico/3.3%20-%20Elaborato%20Piemonte/Varaita.pdf

[S12]https://www.adbpo.it/PAI/3%20-%20Linee%20generali%20di%20assetto%20idraulico%20e%20idrogeologico/3.3%20-%20Elaborato%20Piemonte/Tanaro.pdf

[S13] https://www.arpa.piemonte.it/rischinaturali/tematismi/clima/confronti-storici/dati/dati.html#2.0

[S14] https://www.geoportale.piemonte.it/geonetwork/srv/ita/catalog.search#/metadata/arlpa_to:12.01.01-D_2011-06-21-11:30

[S15]https://www.arpa.piemonte.it/export/sites/default/tematismi/clima/confronti-storici/dati/metodologia.pdf

[S16] https://www.arpa.piemonte.it/rischinaturali/tematismi/clima/rapporti-di-analisi/annuale.html

[S17]https://library.wmo.int/viewer/39629?medianame=wmo_1090_en_#page=13&viewer=picture&o=bookmarks&n=0&q=

[S18] https://www.regione.piemonte.it/web/sites/default/files/media/documenti/2018-11/ai05_varaita_0.pdf

[S19] https://www.regione.piemonte.it/web/sites/default/files/media/documenti/2018-11/ai06_maira_0.pdf

[S20]file:///C:/Users/user/Dropbox%20(Politecnico%20Di%20Torino%20Studenti)/PC/Downloads/TesiMonzaFabio_Cal_FEST_Tanaro.pdf

8. Bibliography

Ali, E., et al. "Cross-Chapter Paper 4: Mediterranean Region. In: Climate Change 2022: Impacts, Adaptation and Vulnerability. Contribution of Working Group II to the Sixth Assessment Report of the Intergovernmental Panel on Climate Change:[H.-O. Pörtner, DC Roberts, M. Tignor, ES Poloczanska, K. Mintenbeck, A. Alegría, M. Craig, S. Langsdorf, S. Löschke, V. Möller, A. Okem, B. Rama (eds.)]." IPCC, Cambridge, United Kingdom and New York, NY, USA (2022).

Allen, Richard G. "Crop evapotranspiration." FAO irrigation and drainage paper 56 (1998): 60-64.

Arpa Piemonte, Dipartimento Rischi Naturali e Ambientali e Dipartimento Sistemi Previsionali e Regione Piemonte, Direzione Ambiente, Energia e Territorio, «Analisi del clima regionale del periodo 1981-2010 e tendenze negli ultimi 60 anni». Torino, giugno 2020 [1]. https://www.regione.piemonte.it/web/sites/default/files/media/documenti/2021 02/analisi_clima_regionale_1981-2010.pdf

Baronetti, Alice, et al. "A weekly spatio-temporal distribution of drought events over the Po Plain (North Italy) in the last five decades." International Journal of Climatology 40.10 (2020): 4463-4476.

Baronetti, Alice, et al. "Future droughts in northern Italy: high-resolution projections using EURO-CORDEX and MED-CORDEX ensembles." Climatic Change 172.3-4 (2022): 22.

Beguería, Santiago, et al. "Standardized precipitation evapotranspiration index (SPEI) revisited: parameter fitting, evapotranspiration models, tools, datasets and drought monitoring." International journal of climatology 34.10 (2014): 3001-3023.

Dracup, John A., Kil Seong Lee, and Edwin G. Paulson Jr. "On the definition of droughts." Water resources research 16.2 (1980): 297-302.

Falzoi, Simone, et al. "Hydrological drought analysis in Continental Temperate and Mediterranean environment during the period 1981-2017." Italian Journal of Agrometeorology 24.3 (2019): 13-23.

Fang, Wei, et al. "Identifying drought propagation by simultaneously considering linear and nonlinear dependence in the Wei River basin of the Loess Plateau, China." Journal of Hydrology 591 (2020): 125287.

Fratianni, Simona, and Fiorella Acquaotta. "The climate of Italy." Landscapes and landforms of Italy (2017): 29-38.

Guttman, Nathaniel B. "Comparing the palmer drought index and the standardized precipitation index 1." JAWRA Journal of the American Water Resources Association 34.1 (1998): 113-121.

Hakam, Oualid, et al. "Spatiotemporal evolution of droughts and their teleconnections with large-scale climatic indices in the Lower Sebou Basin in northwestern Morocco." Acta Geographica Slovenica 62.2 (2022).

Hanel, Martin, et al. "Revisiting the recent European droughts from a long-term perspective." Scientific reports 8.1 (2018): 9499.

Haslinger, Klaus, and Günter Blöschl. "Space-time patterns of meteorological drought events in the European Greater Alpine Region over the past 210 Years." Water Resources Research 53.11 (2017): 9807-9823.

Hargreaves, George H., and Zohrab A. Samani. "Reference crop evapotranspiration from temperature." Applied engineering in agriculture 1.2 (1985): 96-99.

Kim, Cornelis Pieter. The water budget of heterogeneous areas: impact of soil and rainfall variability. Kim, 1995.

Konapala, Goutam, and Ashok Mishra. "Quantifying climate and catchment control on hydrological drought in the continental United States." Water Resources Research 56.1 (2020): e2018WR024620.

Kundzewicz, Zbigniew W., and Zdzislaw Kaczmarek. "Coping with hydrological extremes." Water International 25.1 (2000): 66-75.

MAETENS, Willem, et al. "The European Drought Observatory for Resilience and Adaptation (EDORA)." (2024)

McMahon, T. A., et al. "Estimating actual, potential, reference crop and pan evaporation using standard meteorological data: a pragmatic synthesis." Hydrology and Earth System Sciences 17.4 (2013): 1331-1363.

McKee, Thomas B., Nolan J. Doesken, and John Kleist. "The relationship of drought frequency and duration to time scales." *Proceedings of the 8th Conference on Applied Climatology*. Vol. 17. No. 22. 1993.

Ojara, Moses A., et al. "Evaluation of drought, wet events, and climate variability impacts on maize crop yields in East Africa during 1981–2017." *International Journal of Plant Production* 16.1 (2022): 41-62.

Palmer, W. C., 1965: Meteorological droughts. U.S. Department of Commerce, Weather Bureau Research Paper 45, 58 pp

Pavan, Valentina, et al. "High resolution climate precipitation analysis for north-central Italy, 1961–2015." *Climate Dynamics* 52 (2019): 3435-3453.

Priestley, Charles Henry Brian, and Robert Joseph Taylor. "On the assessment of surface heat flux and evaporation using large-scale parameters." Monthly weather review 100.2 (1972): 81-92.

Searcy, J. K. "Flow-duration curves: Water Supply Paper 1542-A." *US Geological Survey, Reston, VA* (1959).

Sheffield, Justin, and Eric F. Wood. "Projected changes in drought occurrence under future global warming from multi-model, multi-scenario, IPCC AR4 simulations." *Climate dynamics* 31 (2008): 79-105.

Stagge, James H., et al. "Standardized precipitation-evapotranspiration index (SPEI): Sensitivity to potential evapotranspiration model and parameters." *Hydrology in a changing world*. Vol. 363. 2014.

Straffelini, Eugenio, and Paolo Tarolli. "Climate change-induced aridity is affecting agriculture in Northeast Italy." Agricultural Systems 208 (2023): 103647.

Tallaksen, Lena M., and Henny AJ Van Lanen, eds. "Hydrological drought: processes and estimation methods for streamflow and groundwater." (2004).

Tirivarombo, Sithabile, D. Osupile, and Peter Eliasson. "Drought monitoring and analysis: standardised precipitation evapotranspiration index (SPEI) and standardised precipitation index (SPI)." *Physics and Chemistry of the Earth, Parts A/B/C* 106 (2018): 1-10.

Van Lanen, Henny AJ. "Drought propagation through the hydrological cycle." *IAHS publication* 308 (2006): 122.

Van Loon, Anne F., and Henny AJ Van Lanen. "A process-based typology of hydrological drought." *Hydrology and Earth System Sciences* 16.7 (2012): 1915-1946.

Van Loon, Anne Frederike. *On the Propagation of Drought.: How Climate and Catchment Characteristics Influence Hydrological Drought Development and Recovery*. Wageningen University and Research, 2013.

Van Loon, A. F., and G. J. J. O. H. Laaha. "Hydrological drought severity explained by climate and catchment characteristics." *Journal of hydrology* 526 (2015): 3-14.

Van Loon, Anne F. "Hydrological drought explained." Wiley Interdisciplinary Reviews: Water 2.4 (2015): 359-392.

Vicente-Serrano, Sergio M., and Juan I. López-Moreno. "Hydrological response to different time scales of climatological drought: an evaluation of the Standardized Precipitation Index in a mountainous Mediterranean basin." *Hydrology and earth system sciences* 9.5 (2005): 523-533.

Vicente-Serrano, Sergio M., Santiago Beguería, and Juan I. López-Moreno. "A multiscalar drought index sensitive to global warming: the standardized precipitation evapotranspiration index." *Journal of climate* 23.7 (2010): 1696-1718.

Vicente-Serrano, Sergio M., et al. "Accurate computation of a streamflow drought index." *Journal of Hydrologic Engineering* 17.2 (2012): 318-332.

Vogel, Johannes, et al. "Increasing compound warm spells and droughts in the Mediterranean Basin." *Weather and Climate Extremes* 32 (2021): 100312.

Wang, Qianfeng, et al. "Temporal-spatial characteristics of severe drought events and their impact on agriculture on a global scale." *Quaternary International* 349 (2014): 10-21.

Wang, Wen, et al. "Propagation of drought: from meteorological drought to agricultural and hydrological drought." *Advances in Meteorology* 2016 (2016).

Wilhite, Donald A. "Drought assessment, management, and planning: theory and case studies." *(No Title)* (1994).

Wilhite, D., ed.: Drought: A Global Assessment, Vol I & II, Routledge Hazards and Disasters Series, Routledge, London, UK, 2000

Yevjevich, Vujica M. *Objective approach to definitions and investigations of continental hydrologic droughts, An*. Diss. Colorado State University. Libraries, 1967.

Zambreski, Zachary Todd. A statistical assessment of drought variability and climate prediction for Kansas. Diss. Kansas State University, 2016.